Non-canonical contribution of human Dicer helicase domain in antiviral innate immune response

Morgane Baldaccini, Léa Gaucherand, Béatrice Chane-Woon-Ming, Mélanie Messmer, Floriane Gucciardi, Sébastien Pfeffer*

Université de Strasbourg, Architecture et Réactivité de l'ARN, Institut de Biologie Moléculaire et Cellulaire du CNRS, 67000 Strasbourg, France

* To whom correspondence should be addressed: s.pfeffer@ibmc-cnrs.unistra.fr

ABSTRACT

In mammalian somatic cells, the relative contribution of RNAi and the type I interferon response during viral infection is unclear. The apparent inefficiency of antiviral RNAi might be due to self-limiting properties and mitigating co-factors of the key enzyme Dicer. In particular, the helicase domain of human Dicer appears to be an important restriction factor of its activity. We studied the involvement of several helicase-truncated mutants of human Dicer in the antiviral response. All deletion mutants displayed a PKR-dependent antiviral phenotype against certain viruses and one of them, Dicer N1, acted in a complete RNAi-independent manner. Transcriptomic analyses showed that many genes from the interferon and inflammatory response were upregulated in Dicer N1 expressing cells. We could show that some of these genes appear to be controlled by NF-kB and that blocking this pathway abrogated the antiviral phenotype of Dicer N1. Our findings highlight the crosstalk between Dicer, PKR, and the NF-kB pathway, and suggest that human Dicer may have repurposed its helicase domain to prevent basal activation of antiviral and inflammatory pathways.

KEYWORDS

Dicer/Innate immunity/NF-kB/RNAi/Virus

31 **INTRODUCTION**

32 RNAi is an evolutionary conserved cellular defense mechanism against invading nucleic acids.
33 It is based on the detection and cleavage of a trigger double-stranded (ds) RNA by Dicer, a type
34 III ribonuclease. The resulting small interfering (si) RNAs serve as guides for effector
35 Argonaute proteins that will act on target RNAs in a sequence specific manner (Meister &
36 Tuschl, 2004). By its nature, RNAi has been shown to be a prominent defense mechanism
37 against viruses in plant and invertebrate organisms (Guo *et al*, 2019; tenOever, 2016), but its
38 exact contribution to the innate antiviral response in mammals remains to be firmly established.
39 Indeed, several studies failed to identify virus-derived siRNAs in infected mammalian somatic
40 cells (Girardi *et al*, 2013; Backes *et al*, 2014; Parameswaran *et al*, 2010). It was also reported
41 that molecular mechanisms, such as poly-ADP-ribosylation of AGO2, could prevent the
42 activation of RNAi upon viral infection (Seo *et al*, 2013) or that when viral siRNAs did
43 accumulate, they were inefficiently loaded into Argonaute proteins (Tsai *et al*, 2018). However,
44 antiviral RNAi does appear to be active in specific conditions, in particular in pluripotent stem
45 cells (Maillard *et al*, 2013). It also seems to be incompatible with other innate immune defense
46 pathways that rely on the type I interferon response (IFN-I). As a result, certain studies have
47 shown that inactivating the IFN-I response allows RNAi to take over. The pattern recognition
48 receptors that are inactivated in these studies are members of the RIG-I like receptor (RLR)
49 family and they also recognize dsRNA (Ahmad & Hur, 2015; Pichlmair & Reis e Sousa, 2007).
50 However, as opposed to Dicer, they do not act by cleaving dsRNA but rather by inducing a
51 phosphorylation cascade that will ultimately result in the production of the autocrine- and
52 paracrine-acting interferon α and ß cytokines followed by the transcriptional activation of
53 hundreds of interferon stimulated genes (ISGs) (Ivashkiv & Donlin, 2014). Thus, in mammalian
54 somatic cells deficient for MAVS or IFNAR, the production of long-dsRNA-derived siRNAs
55 can be detected and are shown to be dependent on Dicer activity (Maillard *et al*, 2016). Besides,

56 the RLR LGP2 has been shown to directly interact with Dicer, blocking siRNA production and
57 along with TRBP preventing the correct miRNA maturation (Takahashi *et al*, 2018b, 2018a;
58 van der Veen *et al*, 2018). Finally, a recent study showed that the IFN-induced adenosine
59 deaminase ADAR1 could compete with RNAi to act on dsRNA accumulating during a viral
60 infection (Uhl *et al*, 2023). Thus, in mammalian cells, RNAi seems to be functionally
61 incompatible with other innate immune mechanisms, which are suggested to tone down Dicer
62 involvement in the antiviral response.

63 One interesting observation is that the amino-terminal helicase domain is quite conserved
64 between RLRs and Dicer, which might indicate a functional replacement during evolution
65 (Baldaccini & Pfeffer, 2021). In mammalian Dicer, the helicase domain exerts some molecular
66 constraints that limit Dicer's cleavage processivity on long dsRNA molecules (Ma *et al*, 2008).
67 Accordingly, a synthetic Dicer lacking the first two domains of the helicase, Hel1 and Hel2i,
68 and named Dicer N1 displays better cleavage properties of an artificial dsRNA than the full-
69 length version of Dicer (Kennedy *et al*, 2015). More recently, a naturally occurring isoform of
70 Dicer, lacking the Hel2i domain, has been identified in human stem cells and shown to possess
71 some antiviral properties in an RNAi-dependent manner (Poirier *et al*, 2021). Similarly, a Hel1-
72 truncated version of Dicer, coined Dicer^{O}, is specifically expressed in mouse oocytes and is
73 better adapted to cleave long dsRNA molecules than pre-miRNAs (Flemr *et al*, 2013).
74 Uncovering the structure of Dicer^{O} isoform revealed that the N-terminal part of the helicase
75 domain plays an important role for the correct positioning of the pre-miRNA and that removing
76 it potentially increases the affinity for longer dsRNA structures (Zapletal *et al*, 2022). On top
77 of having a molecular self-limiting effect, this helicase domain also allows Dicer to interact
78 with proteins that regulate its activity. We have recently shown that during Sindbis virus (SINV)
79 infection the helicase domain of human Dicer specifically interacts with proteins that are
80 involved in the IFN-I response such as PACT, the RNA helicase DHX9, ADAR1 and the

81 dsRNA-activated protein kinase PKR (Montavon *et al*, 2021). In addition, we reported in the
82 same study that the expression of the helicase-truncated Dicer N1 confers a strong antiviral
83 activity against SINV, and that this phenotype is dependent on the presence of PKR. Similarly,
84 another study shows a genetic link between Dicer and PKR in mouse embryonic stem cells and
85 proposes that Dicer can hinder PKR activity in a non-canonical manner (Gurung *et al*, 2021).
86 Dicer thus seems to have an additional antiviral activity linked to PKR that is limited by its
87 helicase domain.

88 In this study, we sought to uncover the mechanism underlying Dicer N1 antiviral
89 activity. By using HEK293T NoDice cells (Bogerd *et al*, 2014) stably expressing either Dicer
90 WT or N1, we showed that Dicer N1 cells are more resistant than Dicer WT cells to infection
91 with alphaviruses SINV and Semliki forest virus (SFV), and human enterovirus 71 (EV71).
92 However, this antiviral effect was virus-dependent, as Dicer N1 had no impact on vesicular
93 stomatitis virus (VSV) infection, and we even observed a pro-viral effect of Dicer N1 on SARS-
94 CoV-2 infection. Interestingly, we found that the antiviral effect of Dicer N1 is RNAi-
95 independent, as cells expressing a catalytically inactive Dicer N1 were equally protected against
96 SINV infection. We also tested other helicase-truncated mutants of Dicer and observed that
97 individual deletion of each subdomain (Hel1, Hel2i or Hel2) also conferred an antiviral property
98 to Dicer. However, as opposed to Dicer N1, this phenotype appeared to be partially due to
99 RNAi. Nevertheless, all of the helicase-deletion mutants also required the presence of PKR to
100 maintain their antiviral effect. We thus focused our investigations on the implication of PKR in
101 the phenotype of Dicer N1 and showed that it is required for its antiviral activity independently
102 from its kinase function. Transcriptomic analysis of mock- or SINV-infected cells uncovered
103 that Dicer N1 expressing cells have a higher basal expression of a large subset of genes,
104 including a number that are involved in the antiviral response. We further showed that those
105 genes are under the control of transcription factors such as STAT1, STAT2 and NF-kB/p65.

106 Finally, we confirmed the importance of the latter pathway in the phenotype of Dicer N1 cells
107 by alleviating the antiviral effect in cells treated with a chemical inhibitor of NF-kB. Based on
108 these results, we propose that one reason for human Dicer to have maintained a self-limiting
109 helicase domain is to prevent basal activation of antiviral and inflammatory pathways.
110

111 **RESULTS**

112 **Effect of Dicer N1 expression on SINV viral cycle**

113 We previously showed that a partial helicase-deletion mutant of human Dicer expressed in
114 HEK293T NoDice cells presented an antiviral activity against SINV (Montavon *et al*, 2021).
115 We used the two monoclonal cell lines NoDice FHA-Dicer WT #4 and NoDice FHA:Dicer N1
116 #6 (afterward respectively referred to as Dicer WT and Dicer N1 cells) to better characterize
117 the impact of Dicer WT or Dicer N1 expression on SINV viral life cycle. We used a non-
118 modified SINV strain and two different GFP-expressing strains that either express the
119 fluorescent protein from a duplication of the subgenomic promoter (SINV-GFP) or from a
120 fusion with the capsid protein (SINV-2A-GFP) (Thomas *et al*, 2003). The latter expressed GFP
121 at higher levels than the former (Appendix Figure S1A). We infected Dicer WT and Dicer N1
122 cells with increasing MOIs of all three viruses and measured the accumulation of infectious
123 particles by plaque assay 24 hours post-infection (hpi) (Figure 1A). For all viruses, we observed
124 a significant antiviral effect at every MOI in cells expressing Dicer N1 compared to cells
125 expressing Dicer WT. The effect was more pronounced in cells infected with the SINV-2A-
126 GFP, which seems to be attenuated at lower MOIs compared to both other viral strains (Figure
127 1A). We also monitored viral protein accumulation in cells infected for 24h at an MOI of 0.02.
128 In Dicer N1 cells, both the SINV Capsid and GFP proteins accumulated to lower levels, or even
129 below detection limits for SINV-2A-GFP, compared to Dicer WT cells (Figure 1B). We also
130 monitored double-stranded (ds) RNA accumulation during infection as a proxy for viral
131 replication. We used the dsRNA-specific J2 antibody (Richardson *et al*, 2010) to perform
132 immunostaining of cells infected for 24h at an MOI of 0.02 with either of the three SINV strains.
133 Compared to Dicer WT cells, Dicer N1 cells showed a decreased dsRNA accumulation for all
134 three viruses, with a stronger effect for the SINV-2A-GFP virus (Figure 1C). In order to verify
135 that the drop in viral accumulation in Dicer N1 cells was not simply due to a delay in replication,

136 we also measured viral titers by plaque assay in cells infected for 48h with SINV-GFP at two
137 different MOIs (0.01 and 0.001) and for 72h at an MOI of 0.001. In all cases, we could still
138 observe a significant decrease in viral titers in Dicer N1 cells compared to Dicer WT cells
139 (Appendix Figure S1B). Finally, to further confirm the impact of Dicer N1 expression on viral
140 replication, we measured the accumulation of genomic RNA by RT-qPCR in cells infected with
141 SINV-GFP at an MOI of 0.02 for 24h. In agreement with the previous results, Dicer N1 cells
142 showed a very strong decrease of SINV genomic RNA accumulation compared to Dicer WT
143 cells (Figure 1D). In parallel, we also performed semi-quantitative strand-specific RT-PCR on
144 the same samples and observed that the anti-genomic viral RNA accumulated to lower levels
145 in Dicer N1 cells than in Dicer WT cells (Appendix Figure S1C). Collectively, these data
146 indicate that the antiviral activity of Dicer N1 leads to a defect in SINV viral replication.
147
148 **Dicer N1 is antiviral against other positive-strand RNA viruses**
149 To see whether the antiviral activity of Dicer N1 could be generalized to other viruses, we
150 infected Dicer WT and Dicer N1 cells with viruses from different families. We first tested
151 another *Togaviridae* family member, the Semliki forest virus (SFV), and observed a lower viral
152 titer in the supernatants of Dicer N1 cells than in Dicer WT cells infected for 24h at an MOI of
153 1.10^{-4} (Figure 2A, top panel). In addition, dsRNA accumulation, as assessed by J2
154 immunostaining, was barely detectable in Dicer N1 cells, whereas it was very high in Dicer WT
155 cells (Figure 2A, bottom panel). We then infected Dicer WT and N1 cells at an MOI of 0.1 with
156 a (+) RNA virus from the *Picornaviridae* family, human EV71, and measured viral titer in the
157 supernatant by TCID50 at 24 hpi. We observed that the EV71 titer was again lower in Dicer
158 N1 compared to WT cells (Figure 2B, top panel). J2 immunostaining also confirmed a lower
159 accumulation of dsRNA in Dicer N1 cells compared to WT cells (Figure 2B, bottom panel).
160 We also tested the effect of Dicer N1 on a single-stranded negative-sense RNA virus from the

161 *Rhabdoviridae* family, *i.e.* vesicular stomatitis virus (VSV). We infected Dicer WT and N1
162 cells at an MOI of 1.10^{-5} for 24h with an engineered VSV expressing the GFP protein and
163 titrated the virus in the supernatant by plaque assay. We did not detect any significant difference
164 in viral titers between Dicer WT and N1 cells (Figure 2C, top panel). As previously reported
165 (Weber *et al*, 2006), we were not able to detect dsRNA accumulation by J2 immunostaining, in
166 either Dicer WT or N1 cells infected with VSV-GFP. Since dsRNA is a canonical Dicer
167 substrate upon infection, this result indicates that the absence of dsRNA during VSV infection
168 might prevent the activation and antiviral activity of Dicer N1.

169 Finally, we infected the two cell lines with the single-stranded positive-sense RNA virus
170 Severe Acute Respiratory Syndrome Coronavirus 2 (SARS-CoV-2). To be able to use this virus
171 in the HEK293T cells we work with, we first transduced them with a lentiviral vector expressing
172 human ACE2 (hACE2), which is an essential receptor for SARS-CoV-2 infection (Hoffmann
173 *et al*, 2020). We verified hACE2 expression by western blot with a specific antibody (Figure
174 2D). We infected both hACE2-expressing Dicer WT and Dicer N1 cells with SARS-CoV-2 at
175 an MOI of 1.10^{-3} for 48h, and measured viral nucleocapsid expression by western blot analysis.
176 Nucleocapsid expression could be detected in both Dicer WT and N1 cells and seemed to be
177 slightly higher in the latter (Figure 2E). Then, we measured viral titer in the supernatant by
178 TCID50 at 48 hpi. We observed that the SARS-CoV-2 titer was higher in Dicer N1 compared
179 to WT cells (Figure 2F). We also performed J2 immunostaining on SARS-CoV-2 infected cells,
180 and saw that dsRNA was detected equally well in both Dicer WT and N1 cells (Appendix Figure
181 S2A). Finally, we also measured viral RNA accumulation by RT-qPCR, and saw that both
182 ORF1a and Spike RNAs accumulated to higher levels in Dicer N1 than in Dicer WT cells,
183 although the increase was not significant for Spike RNA (Appendix Figure S2B).

184 Altogether, these last results suggest that Dicer N1 expression can have an antiviral effect
185 for two different (+) RNA viruses (SFV and EV71), and a proviral effect for a third one (SARS-

186 CoV-2). This antiviral property does not seem to be active in the case of a (-) RNA virus, VSV,
187 which might be related in this case to the difference in dsRNA accessibility.
188
189 **RNA interference is not involved in Dicer N1 phenotype**
190 We showed that Dicer N1 expression prevents the accumulation of viral genomic and
191 antigenomic RNA during SINV infection and of dsRNA during SINV, SFV and EV71
192 infection. Since it was previously shown that Dicer N1 was more active than Dicer WT to cleave
193 an artificial dsRNA into siRNAs (Kennedy *et al*, 2015), we first hypothesized that the
194 ribonuclease activity of Dicer N1 was responsible for its antiviral activity. To test this
195 hypothesis, we therefore used an affinity-based purification approach (Hauptmann *et al*, 2015)
196 to isolate Ago-associated small RNAs from Dicer WT or N1 cells infected with SINV-GFP at
197 an MOI of 0.02 for 24h and deep-sequenced them. We first mapped the reads to the human and
198 SINV-GFP genomes and observed that the vast majority of small RNAs had a cellular origin
199 (Figure EV1A). Only 0.2 to 1.2% of sequences could be mapped to the viral genome.
200 Interestingly, the percentage of viral reads was four-to-five-fold lower in Dicer N1 cells than in
201 WT cells. We further analyzed the viral reads and determined their size distribution. Small
202 RNAs mapped to both viral genomic and antigenomic RNAs, with a bias in favor of the former,
203 and showed a peak at 22 nt, consistent with a Dicer-mediated cleavage (Figure 3A, Appendix
204 Figure S3A). However, there was no real difference in size distribution or strand origin between
205 Dicer WT and N1 cells. Small RNAs mapped to the viral genome showed a strong enrichment
206 at the 5' extremity of the genomic RNA in both Dicer WT and N1 cells (Figure 3B, Appendix
207 Figure S3B), in agreement with previous reports (Kong *et al*, 2023; Zhang *et al*, 2021). The
208 relative number of reads that mapped to both strands of the viral RNA was similar in Dicer WT
209 and N1 cells. It therefore appears that both Dicer WT and Dicer N1 are competent for the
210 generation of what looks like viral siRNAs that are loaded in Argonaute proteins, but we did

211 not see an increase in their number in Dicer N1 expressing cells. At this stage, we therefore
212 cannot say that the observed antiviral phenotype of Dicer N1 is linked to a stronger RNAi
213 activity. We also checked whether the expression of Dicer N1 had an impact on the miRNA
214 profile. The analysis of the 50 most abundant miRNAs retrieved in the sequencing data did not
215 reveal striking differences between Dicer WT and N1 cells (Figure EV1B). Similarly, the global
216 analysis of all miRNAs identified in the libraries showed that some lowly abundant miRNAs
217 were differentially expressed, but when looking at miRNAs expressed at a level sufficient for
218 exerting a physiologically relevant effect the observed differences were minimal (Figure
219 EV1C).

220 To further confirm that the Dicer N1 phenotype was independent of its role in RNAi, we
221 generated a catalytic-deficient version of Dicer N1 by introducing mutations in both of its
222 RNAse III domains (Figure 3C). As previously, we used the HEK293T NoDice 2.20 cell line
223 (Bogerd *et al*, 2014) that we transduced with lentiviral vectors expressing a Flag-HA-tagged
224 version of Dicer N1 with mutations in the catalytic domain (N1-CM). We then selected a clone,
225 NoDice FHA:Dicer N1-CM #2.17 (afterwards called Dicer N1-CM), that expressed Dicer at
226 levels similar to the Dicer WT and Dicer N1 cell lines previously generated (Figure 3D). The
227 levels of PKR and TRBP were mostly similar to the ones in Dicer N1 cells. By blotting AGO2
228 in these cell lines, we observed that it was absent in the Dicer N1-CM cells, which is expected
229 for a miRNA-free Argonaute protein and is consistent with previous observations (Gibbings *et*
230 *al*, 2012). We confirmed the defect in miRNA processing in the Dicer N1-CM cells by
231 measuring miR-16 accumulation by northern blot analysis. As expected, we saw no mature
232 miR-16 form and the accumulation of its precursor in Dicer N1-CM cells (Figure 3E). We then
233 infected Dicer WT, N1 and N1-CM cells with SINV-GFP at an MOI of 0.02 for 24h and
234 measured the infection rate by western blot analysis and plaque assay. The level of the capsid
235 protein was strongly reduced in both Dicer N1 and Dicer N1-CM cells compared to Dicer WT

236 cells (Figure 3F). To confirm these observations, we titrated the infectious viral particles in the
237 supernatant and observed a strong and significant decrease of viral titers in both Dicer N1 and
238 Dicer N1-CM compared to Dicer WT cells (Figure 3G). To rule out any clone-dependent effect,
239 we performed the same experiment in polyclonal cells expressing Dicer WT, N1 or N1-CM.
240 As for the monoclonal cell lines, Dicer N1 and N1-CM cells displayed a drop in Capsid protein
241 accumulation compared to Dicer WT cells (Figure EV1D). Accordingly, the viral titer was
242 strongly reduced in Dicer N1 and N1-CM cells compared to Dicer WT cells (Figure EV1E).
243 We showed previously that Dicer N1 could no longer interact with the Dicer co-factors TRBP
244 and PACT and with the kinase PKR (Montavon *et al*, 2021). Thus, we verified by co-
245 immunoprecipitation the interaction of Dicer N1-CM with these proteins. The results confirmed
246 that Dicer N1-CM behaved similarly to Dicer N1 regarding the loss of these interactions (Figure
247 EV1F).

248 Taken together, these results clearly show that the antiviral phenotype of Dicer N1 does
249 not depend on its catalytic activity, and therefore on RNAi, which is in agreement with our
250 previous observations that the antiviral effect of Dicer N1 did not depend on AGO2 (Montavon
251 *et al*, 2021).

252

253 **Impact of Dicer helicase subdomain deletions on viral infection**

254 The region deleted in Dicer N1 contains both the Hel1 and Hel2i domains of the helicase, and
255 was designed based on the presence of an alternative initiation codon at this position (Kennedy
256 *et al*, 2015). Other deletion mutants have been reported in the literature, such as the rodent-
257 specific Dicer^{O}, which is naturally expressed in oocytes (Flemr *et al*, 2013). Similar to Dicer
258 N1, this truncated Dicer was shown to be more potent at generating siRNAs, and was further
259 functionally and structurally studied under the name Dicer ΔHel1 (Zapletal *et al*, 2022). Finally,
260 another Dicer isoform has been recently reported in human embryonic stem cells and was

261 coined antiviral Dicer (AviD) for its RNAi-related antiviral property against different viruses
262 (Poirier *et al*, 2021). This isoform lacks the Hel2i connector domain. To test the behavior of all
263 these deletion mutants during SINV infection, we generated lentiviral constructs expressing a
264 Flag-HA tagged version of Dicer ΔHel1, ΔHel2i and a version lacking the third helicase domain
265 ΔHel2 (Figure 4A). We used these lentiviral constructs, as well as catalytically inactive versions
266 of them called CM, to generate monoclonal NoDice cell lines. We first verified the correct
267 expression of the Dicer isoforms and checked their impact on AGO2, TRBP and PKR
268 expression (Figure EV2A). We also checked that the catalytically inactive versions of the
269 constructs were indeed impaired in miRNA biogenesis by measuring miR-16 expression by
270 northern blot analysis (Figure EV2B). We then infected cells expressing Dicer WT, ΔHel1,
271 ΔHel2i, ΔHel2 or their catalytically inactive versions (CM) with SINV-GFP at an MOI of 0.02
272 for 24h and monitored Capsid protein accumulation by western blot analysis. The levels of
273 Capsid were lower in all cell lines expressing helicase truncated versions of Dicer compared to
274 Dicer WT cells, but seemed to go up when the RNAse III activity was mutated, although slightly
275 less so in the case of ΔHel2 (Figure 4B). To really assess the impact of the expression of these
276 mutants on viral production, we titrated by plaque assay the supernatants of the previous
277 experiment, using Dicer N1 cells as control. We observed that expression of all helicase
278 deletion mutants, Dicer ΔHel1, ΔHel2i and ΔHel2, resulted in a significant drop in viral titer,
279 although slightly less than in Dicer N1 expressing cells, and that this effect was lost in cells
280 expressing the CM versions of the mutants (Figure 4C). Altogether, these results suggest that
281 deleting any helicase subdomain confers an antiviral activity to human Dicer.

282 We previously showed that Dicer N1 antiviral phenotype was dependent on the
283 expression of PKR (Montavon *et al*, 2021). We therefore tested the impact of the expression of
284 the various helicase deletion mutants on viral infection in NoDice cells compared to
285 NoDiceΔPKR cells. We transduced the aforementioned cell lines with Dicer WT, N1, ΔHel1,

286 ΔHel2i and ΔHel2 to generate polyclonal cell lines. We again made sure that these cell lines
287 expressed the different Dicer constructs as well as similar levels of interacting proteins such as
288 AGO2 and TRBP (Figure EV2C), and that they were also competent for miRNA production
289 (Figure EV2D). We then infected all those cell lines with SINV-GFP at an MOI of 0.02 for 24h
290 and measured the expression of the Capsid protein by western blot analysis. We could observe
291 a lower accumulation in NoDice cells transduced with Dicer ΔHel1, ΔHel2 and ΔHel2i
292 compared to cells transduced with Dicer WT (Figure 4D), although the effect was less evident
293 for cells expressing Dicer ΔHel2. On the contrary, in NoDiceΔPKR cells transduced with Dicer
294 ΔHel1, ΔHel2 and ΔHel2i, we did not observe such a strong decrease in Capsid protein levels.
295 We then determined the viral titers produced upon SINV-GFP infection of NoDice and
296 NoDiceΔPKR cells expressing Dicer WT, N1, ΔHel1, ΔHel2i or ΔHel2. While we confirmed
297 the antiviral effect of the helicase deletion mutants compared to the WT Dicer in NoDice cells,
298 we saw that this effect was completely abrogated in NoDiceΔPKR cells (Figure 4E). We also
299 performed an infection kinetic using SINV-GFP at an MOI of 2 in NoDice and NoDiceΔPKR
300 cells expressing Dicer WT or the different helicase deletion mutants and monitored GFP
301 fluorescence every hour for 24h. The results, shown in Figure 4F, confirmed that the percentage
302 of GFP positive cells increased slower in NoDice cells expressing the different helicase mutants
303 than in the ones expressing Dicer WT, with a stronger effect in the presence of Dicer N1 or
304 Dicer ΔHel2i. In NoDiceΔPKR cells, the difference in GFP positive cells accumulation over
305 time was less marked between conditions and the differences were not significant (Figure 4F).
306 We confirmed these observations by performing a plaque assay in the same conditions at 12
307 and 16 hpi. The viral titers were significantly lower at both time points in NoDice cells
308 expressing Dicer helicase mutants than in the ones expressing Dicer WT, while this was not the
309 case in NoDiceΔPKR cells, except for a modest effect in NoDiceΔPKR expressing Dicer
310 ΔHel2i at 16 hpi (Figure EV2E). We can therefore conclude that the antiviral phenotype of

311 Dicer N1 can also be observed with smaller deletion mutants lacking individual subdomains of
312 the helicase. However, as opposed to Dicer N1, it seems that in the case of Dicer ΔHel1, ΔHel2i
313 or ΔHel2, this phenotype is dependent on the catalytic activity of Dicer, and thus is likely RNAi-
314 dependent. Surprisingly, the antiviral phenotype of Dicer ΔHel1, ΔHel2i or ΔHel2 is also lost
315 in cells that do not express PKR, indicating that for these mutants as well, RNAi is not the sole
316 explanation for their behavior. We thus decided to look more into the role of PKR.
317
318 **PKR, but not its catalytic activity, is directly involved in the Dicer N1 phenotype**
319 As shown above, the antiviral phenotype of Dicer helicase mutants seems to be strictly
320 dependent on the expression of PKR. To validate the implication of PKR, we decided to re-
321 express it in NoDiceΔPKR cells to see whether this would complement the antiviral phenotype
322 of Dicer N1. We also designed mutant versions of PKR as indicated in Figure 5A. These
323 mutants are: K296R, which is not able to bind ATP, homodimerize, autophosphorylate or
324 phosphorylate its targets (Dey *et al*, 2005), and T451A, which is still able to form homodimers
325 but has lost its ability to autophosphorylate the T451 residue and to phosphorylate its targets
326 (Taylor *et al*, 2001). We first transduced constructs expressing MYC:CTRL, MYC:PKR WT,
327 MYC:PKR K296R or MYC:PKR T451A in NoDiceΔPKR FHA:Dicer WT cells and infected
328 them with SINV-GFP at an MOI of 0.02 for 24h. We analyzed the expression of PKR and its
329 phosphorylated form by western blot analysis, which confirmed that all constructs were
330 expressed at high levels, but only WT PKR could be phosphorylated upon SINV infection
331 (Figure 5B). Interestingly, there was some basal level of phosphorylated PKR in the mock-
332 infected cells expressing WT PKR, which could be due to a higher expression of PKR in
333 transduced cells compared to WT cells. In terms of viral capsid accumulation, no real difference
334 could be detected between the different conditions (Figure 5B). We measured viral particle
335 production by plaque assay in SINV-GFP infected cells, and could not detect any difference

336 between samples (Figure 5C). This result indicates that in the presence of Dicer WT, expression
337 of a WT or inactive mutant PKR has no significant impact on SINV infection. We then
338 transduced the same MYC:CTRL or PKR constructs as above in NoDiceΔPKR FHA:Dicer N1
339 cells and performed the same analysis after infection with SINV-GFP. The western blot analysis
340 was consistent with the previous one and confirmed the correct expression of the PKR
341 constructs as well as the activation of only the WT PKR version (Figure 5D). However, we
342 noted a small reduction of Capsid protein accumulation in cells expressing MYC:PKR WT,
343 K296R or T451A compared to the MYC:CTRL condition (Figure 5D). This was confirmed by
344 the plaque assay analysis that revealed a significant drop in viral titer in NoDiceΔPKR Dicer
345 N1 cells expressing WT or inactive PKR compared to cells expressing the negative control
346 (Figure 5E). We could thus restore the antiviral phenotype of Dicer N1 by re-expressing PKR
347 in cells where its expression was ablated. Interestingly, this did not require a catalytically active
348 or homodimerization competent PKR since the same complementation could be observed with
349 two different mutants that were both unable to phosphorylate their substrates. We also tested
350 whether the expression of WT or inactive PKR had an impact on SINV infection in the absence
351 of Dicer. We therefore transduced NoDiceΔPKR FHA:CTRL cells with constructs expressing
352 MYC:CTRL, MYC:PKR WT, K296R or T451A and infected them for 24h with SINV-GFP at
353 an MOI of 0.02. Although we could measure a small effect on Capsid protein expression (Figure
354 EV3A), there was no significant difference in viral titers (Figure EV3B) between conditions,
355 which indicates that the presence of Dicer N1 is required to observe a PKR-dependent antiviral
356 effect. Finally, because we observed that Dicer N1 expressing cells appeared to be more
357 sensitive to SARS-CoV-2 infection, we also tested the effect of removing PKR in this setting.
358 We therefore transduced hACE2 in NoDiceΔPKR cells and then transduced them with
359 FHA:Dicer WT or FHA:Dicer N1 constructs before infecting them with SARS-CoV-2 for 48h
360 at an MOI of 0.001. We verified that these cells expressed ACE2 and the WT or N1 isoforms

361 of Dicer, and monitored viral Nucleocapsid accumulation by western blot analysis (Figure 5F)
362 and viral titers by TCID50 (Figure 5G). While NoDice cells expressing Dicer N1 showed the
363 previously observed increase in viral infection levels compared to Dicer WT cells, we could
364 not observe the same difference in NoDiceΔPKR cells. The infection levels were globally
365 higher in these cells compared to NoDice cells, but we did not observe a further increase in
366 Dicer N1 vs. Dicer WT cells. Overall, these results suggest that the antiviral activity towards
367 SINV or proviral activity towards SARS-CoV-2 of Dicer N1 is linked to PKR, and in the case
368 of the antiviral effect, does not require the canonical activation of PKR through
369 homodimerization and phosphorylation.
370
371 **Expression of Dicer N1 induces major changes in the transcriptome**
372 To decipher the mechanism behind Dicer N1 antiviral property, we performed total RNAseq
373 analysis on both Dicer WT and Dicer N1 cells either mock-infected, infected with SINV-GFP
374 at an MOI of 2 for 12h or infected with SINV-GFP at an MOI of 0.02 for 24h. We first verified
375 the percentage of viral reads in the libraries and observed that it was higher (about 8-fold for
376 the genomic RNA) in Dicer WT than in Dicer N1 cells (Figure EV4A). This confirmed the
377 antiviral effect of Dicer N1 at the level of viral replication. Next, we compared the overall
378 profiles of gene expression in the different conditions (Figure 6A). The analysis identified 5
379 groups of genes according to their expression patterns. The first group was composed of genes
380 overexpressed in N1 cells compared to WT cells. The second one was composed of genes
381 specifically downregulated in WT cells upon infection, whereas the third one represented genes
382 downregulated upon infection in both cell lines. Finally, the fourth and fifth groups comprised
383 genes that are upregulated in both WT and N1 cells or in WT cells only, respectively. The first
384 two groups were of interest as several genes were upregulated in Dicer N1 cells no matter
385 whether there were infected or not. We then performed a differential gene expression analysis

386 of mRNAs using DEseq2 (Love *et al*, 2014) to determine the impact of the infection on the cell
387 transcriptome. The results confirmed that in Dicer WT cells, infection by SINV resulted in
388 major changes in the expression levels of a large number of mRNAs, which were visible both
389 at 12 and 24 hpi (Figure 6B, Figure EV4B). However, in Dicer N1 cells, these changes were
390 substantially more limited at both time points of infection (Figure 6C, Figure EV4B), consistent
391 with the fact that the infection was attenuated in these cells and therefore did not result in a
392 strong cellular response. Strikingly, when we compared the transcriptomes of mock-infected
393 Dicer WT and Dicer N1 cells, we found that there was a large number of up-regulated mRNAs,
394 as well as a smaller number of down-regulated mRNAs (Figure 6D). It seems therefore that the
395 expression of Dicer N1 results in changes at the transcriptional level, so we set out to examine
396 whether any of these perturbations could explain the phenotype we observed in these cells. To
397 determine whether specific clusters of genes were specifically deregulated between Dicer WT
398 and N1 cells, we looked at gene set enrichment analysis (GSEA) against the human Hallmark
399 gene sets, which represent specific well-defined biological states or processes with coherent
400 expression (Figure 6E, Figure EV4C, D). In Dicer N1 cells, gene sets linked to interferon alpha,
401 interferon gamma, inflammatory and NF-kB responses were significantly enriched compared
402 to Dicer WT cells (Figure 6E). When looking at the individual enrichment plots for hallmarks
403 such as IFN alpha, gamma or inflammatory response and TNF alpha signaling via NF-kB, we
404 clearly noticed a strong enrichment score in Dicer N1 vs. Dicer WT mock cells (Figure EV4C).
405 These results uncovered a basal innate immunity signature linked to a subset of genes in Dicer
406 N1 cells. In contrast, gene sets belonging to the same hallmarks (IFN alpha, IFN gamma,
407 inflammatory response and TNF alpha signaling *via* NF-kB) were depleted in Dicer WT
408 infected vs. mock cells (Figure EV4D).

409 Altogether, these results highlight transcriptomic differences in Dicer N1 compared to
410 WT cells in mock and SINV infected cells. Globally, immune-related processes seem to be
411 enriched in Dicer N1 cells compared to WT cells, and this, even in the steady state.
412
413 **Dicer N1 expression increases the activation of immune-related transcription factors**
414 Given the seemingly upregulation of innate immune genes in the Dicer N1 cells, we
415 looked for transcription factors that are known to play important roles in innate immunity and
416 analyzed the expression levels of their target genes in the different samples. We retrieved lists
417 of the known targets of NF-kB/p65, STAT1, STAT2, IRF2 and IRF3 and extracted from these
418 lists genes that were differentially expressed either during infection in Dicer WT or Dicer N1
419 cells, or between mock-infected Dicer WT and Dicer N1 cells. We then computed the
420 cumulative frequencies of de-regulated transcripts by comparing i) Dicer WT SINV-GFP 24hpi
421 vs. Dicer WT mock, ii) Dicer N1 SINV-GFP 24hpi vs. Dicer N1 mock and iii) Dicer N1 mock
422 vs. Dicer WT mock. This analysis was done for NF-kB/p65 (Figure 7A) and STAT2 (Figure
423 7B) targets, which were the ones with the greater changes, but also for IRF2 (Figure EV5A),
424 IRF3 (Figure EV5B) and STAT1 (Figure EV5C) targets. The results indicate first that there are
425 more NF-kB target genes that are regulated upon SINV infection in Dicer WT compared to
426 Dicer N1 cells (see the black vs. red curves in Figure 7A). This was less evident for STAT2
427 targets, probably due to the lower number of genes involved (Figure 7B). Surprisingly, there
428 were significantly more upregulated NF-kB and STAT2 targets when comparing Dicer N1
429 mock to Dicer WT mock than when comparing Dicer WT SINV-infected to Dicer WT mock
430 conditions (see the blue vs. black curves in Figure 7A, B). A global representation in the form
431 of heatmaps for the same sets of genes that are known targets of NF-kB/p65 or STAT2 also
432 allowed to visualize the stronger changes induced by the infection in Dicer WT cells compared
433 to Dicer N1 cells, and that a large number of these targets were more expressed in Dicer N1

434 mock than in Dicer WT mock condition (Figure 7C, D). We also represented DEseq2 results
435 obtained for NF-kB/p65 and STAT2 targets in Dicer WT infected vs mock and Dicer N1 mock
436 vs Dicer WT mock comparisons on volcano plots (Figure EV5D, E). Some of the most up-
437 regulated NF-kB targets are also listed in Figure EV5F. These plots indicate that there are
438 specific NF-kB and STAT2 target genes upregulated in Dicer N1 mock compared to Dicer WT
439 cells that are not differentially expressed in Dicer WT SINV-infected compared to mock cells.
440 We validated the increased expression of some selected target genes by RT-qPCR and
441 could confirm that PTGS2, APOBEC3B, MX1, OAS3, and IFIT3 mRNAs were indeed
442 significantly upregulated in mock-infected Dicer N1 compared to Dicer WT cells (Figure 7E).
443 Conversely, very mild or no expression increase and sometimes a decrease in expression was
444 detected for the selected target genes in Dicer N1 infected compared to mock cells, consistent
445 with the RNAseq analysis (Figure EV5G). Besides, the decrease in mRNA levels observed in
446 WT cells upon infection was expected as SINV blocks RNA Pol II transcription via its nsP2
447 protein (Akhrymuk *et al*, 2018). We also verified whether the observed upregulation of NF-kB
448 targets was accompanied by an increase in basal levels of IFN-I levels in Dicer N1 cells. We
449 measured expression of *IFNß* mRNA by RT-qPCR in Dicer WT and Dicer N1 cells, but
450 although there was a tendency for an increased expression in Dicer N1 cells, it was not
451 significant (Figure 7F). This was not too surprising given the fact that HEK293T cells are
452 known for expressing low levels of IFNß even when stimulated (Ferreira *et al*, 2020).
453 Overall, the transcriptome changes induced by Dicer N1 expression, which we validated
454 for selected transcripts by RT-qPCR, allow us to postulate that these cells are in a pre-activated
455 state that might explain their increased resistance to SINV infection. This state appears to be
456 more a pre-inflammatory state rather than an overall pre-activation of IFN-I response. We
457 therefore decided to follow up on the implication of the NF-kB pathway.
458

459 **The NF-kB pathway is implicated in the antiviral phenotype of Dicer N1**

460 We showed above that the presence of PKR but not its canonical kinase activity was needed for
461 the Dicer N1 antiviral phenotype. It has been reported that PKR can be involved in the
462 activation of the immune response in a non-canonical manner. In particular, PKR has been
463 described as an inducer of NF-kB/p65 transcriptional activity independently of its kinase
464 function (Bonnet *et al*, 2000). Since we also found that targets of NF-kB are induced
465 specifically in Dicer N1 cells, we investigated whether this pathway was involved in the
466 antiviral phenotype of these cells. NF-kB/p65 is known to be phosphorylated once IkBα is
467 released from the complex, which results in NF-kB/p65 activation upon translocation into the
468 nucleus (Christian *et al*, 2016; Kanarek & Ben-Neriah, 2012). We looked at the expression and
469 phosphorylation levels of NF-kB/p65 in Dicer WT and N1 cells during a time course of SINV-
470 GFP infection at an MOI of 2 from 3 to 24 hpi (Figure 8A). In Dicer WT cells, we observed an
471 increase in p65 phosphorylation at 6 hpi, which corresponds to the end of the first replication
472 cycle. However, at 12 hpi the phosphorylation decreased and became undetectable at 24 hpi. In
473 Dicer N1 cells, the level of phosphorylated p65 was already quite elevated in the mock-infected
474 condition and remained high until 12 hpi where it slightly decreased until 24 hpi (Figure 8A).
475 At the same time, we noticed a higher level of NF-kB/p65 protein at both 12 and 24 hpi. To
476 further link the phosphorylation of p65 to a de-regulation of PKR in Dicer N1 cells, we infected
477 NoDiceΔPKR cells expressing FHA:Dicer N1 and transduced with either a MYC:CTRL or a
478 MYC:PKR WT construct and measured the levels of p65, its phosphorylated form and capsid
479 protein by western blot analysis. We confirmed the effect of the lack of PKR on SINV capsid
480 accumulation and observed an increase in phospho-p65 in both mock- and SINV-infected cells
481 only when PKR expression was restored (Figure 8B). The increase in NF-kB activity in Dicer
482 N1 cells expressing PKR could also be validated by measuring expression of its target PTGS2
483 by RT-qPCR (Figure 8C).

484 Given the higher activation levels of p65 in Dicer N1 cells, we then decided to block the
485 NF-kB pathway to test its role during SINV infection. To do so, we used the chemical
486 compound BAY 11-7082, which inhibits IkBα phosphorylation by the IKK kinases and thus
487 prevents NF-kB/p65 activation (Pierce *et al*, 1997). We treated Dicer N1 cells with two
488 different concentrations of BAY 11-7082 during 1h. Then, we infected cells with SINV-GFP
489 at an MOI of 0.02 for 24h and evaluated the impact of the drug treatment on the infection
490 efficiency. As shown in Figure 8D, we observed a dose-dependent decrease in the
491 phosphorylation of p65 in mock-infected cells treated with BAY 11-7082 compound compared
492 to cells treated with DMSO only. Conversely, the level of IkBα was increased in cells treated
493 with the inhibitor compared to the control. These results indicate that the treatment was
494 effective. We further validated that the inhibitor worked as expected by analyzing the mRNA
495 levels of the previously validated NF-kB target PTGS2 by RT-qPCR. In Dicer N1 cells treated
496 with BAY 11-7082, the level of this mRNA was reduced in a dose-dependent manner compared
497 to the control condition (Figure 8E). The effect of the NF-kB inhibitor on viral infection could
498 be visualized first by the increased accumulation of the capsid protein in SINV-GFP infected
499 cells treated with 5 µM of BAY 11-7082 compared to DMSO-treated cells (Figure 8D). Finally,
500 we measured the effect of NF-kB inhibition on viral particle production, and observed a
501 significant increase in viral titers in Dicer N1 cells treated with 5µM of BAY compared to the
502 negative control (Figure 8F). The BAY 11-7082 treatment had no effect on SINV-GFP
503 infection in Dicer WT cells, as assessed by western blot analysis of the capsid protein and by
504 plaque assay (Appendix Figure S4A, B). Overall, these results indicate that by blocking the NF-
505 kB/p65 pathway with BAY 11-7082, the antiviral activity of Dicer N1 can be reverted,
506 suggesting that the antiviral activity of Dicer N1 is partially mediated through the NF-kB/p65
507 pathway.
508

509 **DISCUSSION**

510 In this study, we examined the role played by Dicer during viral infection in human cells. We
511 specifically focused on the importance of its helicase domain, as it is known to play important
512 roles in modulating its activity. Indeed, some of the deletion mutants that we used in our
513 analysis, such as Dicer N1, Dicer ΔHel1 or Dicer ΔHel2i have been reported to display
514 increased RNAi activity directed against either artificial dsRNA substrate or specific viruses
515 (Kennedy *et al*, 2015; Poirier *et al*, 2021; Zapletal *et al*, 2022). Our results confirmed that
516 helicase-truncated Dicer proteins displayed an antiviral phenotype against some, but not all,
517 viruses. While we observed that the catalytic activity of Dicer was involved for some deletion
518 mutants, we also showed that the presence of the PKR protein was an essential feature for the
519 antiviral phenotype of all deletion mutants tested. In particular, the Dicer N1 variant, which was
520 shown to be capable of RNAi activity in cells that did not express PKR (Kennedy *et al*, 2015)
521 was antiviral in our hands only in the presence of PKR, and remained antiviral when rendered
522 catalytically inactive. A link between Dicer and PKR was also proposed in mouse embryonic
523 stem cells where Dicer appears to prevent the PKR-induced IFN-I response (Gurung *et al*,
524 2021). However, no mechanism was proposed, and the authors hypothesized that it might be
525 linked to miRNA production. We do not believe that miRNAs are involved in the phenotype of
526 Dicer N1 since there were no dramatic changes in miRNA profiles induced by its expression.
527 Our data seem to indicate that the PKR-mediated antiviral effect observed in cells expressing
528 helicase-truncated Dicer proteins is dominant over the RNAi-mediated effect. One would
529 expect that RNAi would be more potent when PKR is not expressed since it should compete
530 with Dicer for dsRNA binding. The fact that it is not the case during the antiviral response
531 raises interesting perspectives. Surprisingly, we also observed that expression of Dicer N1 had
532 a proviral effect in the case of SARS-CoV-2, and that this phenotype was also dependent on

533 PKR expression. This observation definitely rules out the involvement of RNAi since the virus
534 levels are increased in this case.

535 PKR is a key effector protein involved in pathways such as apoptosis, autophagy, cell
536 cycle control and immunity (Williams, 1999). Besides its well-known role in translation control
537 *via* phosphorylation of the eIF2α factor (Donnelly *et al*, 2013), it also plays key roles in
538 modulating IFN-I signaling pathways and can negatively regulate STAT1 and STAT3
539 transcriptional activity in a kinase-dependent manner (Raven *et al*, 2006). It has also been
540 involved in the NF-kB pathway, but in this case it can do so both in a catalytic-dependent (Gil
541 *et al*, 2001) and independent way, via the IKK kinase (Bonnet *et al*, 2000; Ishii *et al*, 2001).
542 Here, we showed that Dicer N1 expressing cells had a different transcriptome from Dicer WT
543 expressing cells and showed a significant enrichment of gene sets related to IFN alpha/gamma
544 and inflammatory/NF-kB responses. Specifically, we could identify among the differentially
545 expressed genes a substantial fraction of targets of key immune transcription factors such as
546 STAT2 and NF-kB. We retrieved and validated the differential expression levels for known
547 antiviral effectors such as PTGS2, APOBEC3B or OAS3 (Jiang *et al*, 2008; Lehman *et al*,
548 2022; Manjunath *et al*, 2023; Ryman *et al*, 2002). This observation is reminiscent of other
549 studies that showed that Dicer could be involved in non-RNAi related signaling pathways. For
550 instance, *Drosophila* Dicer-2 can induce the expression of a small antiviral peptide, Vago, in a
551 tissue- and virus-specific manner (Deddouche *et al*, 2008). More recently, plant DCL2 was
552 involved in auto-immunity activation upon *DCL4* loss and in the activation of defense gene
553 expression such as nucleotide-binding domain/leucine-rich repeat immune receptors (Nielsen
554 *et al*, 2023). By measuring expression levels of *IFNβ* mRNA in Dicer N1 expressing cells, we
555 could hypothesize that most of the observed effect results from a de-regulation of the NF-kB
556 pathway without a requirement for cytokine production. We confirmed this hypothesis by
557 treating Dicer N1 expressing cells with an NF-kB inhibitor, which resulted in the abrogation of

558 their antiviral phenotype. We can therefore assume that the transcriptional deregulation of key
559 genes involved in the innate immune response and under the control of NF-kB was responsible
560 for the observed effect on virus infection. Furthermore, the fact that Dicer N1 cells presented
561 increased levels of SARS-CoV-2 infection is also in favor of an involvement of NF-kB
562 signaling. Indeed, SARS-CoV-2 is known to benefit from the upregulation of the inflammatory
563 response, mainly through the NF-kB pathway, which is essential for the replication and
564 propagation of the virus (Nilsson-Payant *et al*, 2021). A very recent study confirmed the
565 proviral role of the NF-kB pathway in SARS-CoV-2 infected lung cells(Bhargava *et al*, 2023).
566 Our study reinforces the non-canonical roles of Dicer in immune signaling pathways and
567 its interplay with other antiviral responses. Dicer helicase domain sequesters PKR away from
568 its conventional signaling function. We showed that Dicer N1 antiviral activity only depends
569 on the presence of PKR but not on its dimerization or catalytic activity. Even though we cannot
570 at this stage formally conclude on the mechanism at play, we can speculate that PKR cofactors
571 TRBP and/or PACT might be involved. Indeed, PKR can be activated by PACT upon stress
572 (Farabaugh *et al*, 2020; Ito *et al*, 1999). Conversely, TRBP can inhibit PKR directly or sequester
573 PACT away from PKR (Chukwurah & Patel, 2018; Daher *et al*, 2009). Since both proteins also
574 interact with Dicer *via* its helicase domain and thus cannot interact with it anymore in the Dicer
575 N1 cells, they are expected to preferentially interact with other partners such as PKR in the
576 Dicer N1 background and they could limit or change its canonical function. This could in theory
577 explain the activation of the NF-kB pathway in a PKR-dependent manner in the presence of a
578 helicase-truncated Dicer. Interestingly, it was previously shown that the NF-kB pathway could
579 promote SINV infection, but only in mature non-dividing neurons (Yeh *et al*, 2019). In the
580 proliferating cell line that we used, we rather showed that the basal activation level of NF-kB
581 in Dicer N1 cells is antiviral. In agreement with this observation, inhibiting NF-kB in Dicer
582 WT cells has no effect on SINV, which is similar to what has been reported in the Yeh *et al*

583 study. Our results therefore indicate that in actively dividing cells, the NF-kB status dictates the
584 fate of SINV infection, and this can be in part controlled by the Dicer isoform expressed. Of
585 course, it remains to be seen whether our observations, which were done in one specific cell
586 line, can be generalized to other cellular systems. In particular, this point is crucial for cells that
587 naturally express isoforms of helicase-truncated Dicer, *i.e.* oocytes and stem cells: it would be
588 important to check whether signaling pathways are deregulated and whether this contributes to
589 the antiviral effect that has been reported for the AviD isoform (Poirier *et al*, 2021).

590 Overall, our study reinforces the idea of a crosstalk between RNAi and other innate
591 immune pathways, in this case NF-kB, and highlights a non-canonical function of human Dicer
592 upon infection (Figure 9). We showed that Dicer helicase domain is linked to the regulation of
593 immune signaling pathways, and can therefore potentially prevent unwanted activation of these
594 pathways. This new function depends on a non-catalytic action of PKR, which can activate the
595 NF-kB pathway, when no longer interacting with Dicer. In turn, depending on the virus, this
596 activity results either in an antiviral or a proviral effect.

597 **MATERIALS & METHODS**

598 **Plasmids, cloning and mutagenesis**

599 N1 DICER, N1-CM DICER, ΔHEL1 DICER and ΔHEL1-CM DICER were generated by PCR
600 mutagenesis from pDONR-DICER described in (Girardi *et al*, 2015). ΔHEL2i and ΔHEL2
601 DICER and their catalytic mutants (CM) were generated by InFusion mutagenesis (Takara Bio)
602 on pDONR-DICER and pDONR-DICER catalytic mutant vectors. pLenti Flag-HA-V5 vector
603 was modified from pLenti6-V5 gateway vector (Thermo Fisher scientific V49610) by Gibson
604 cloning. WT, N1, N1-CM, ΔHEL1, ΔHEL2i, ΔHEL2, ΔHEL1-CM, ΔHEL2i-CM and ΔHEL2-
605 CM DICER from pDONR plasmids were cloned in pLenti flag-HA-V5 by Gateway
606 recombination.

607 pLenti MYC:PKR and pLenti human ACE2 vectors were purchased from VectorBuilder.
608 pLenti MYC:CTRL vector was modified from pLenti MYC:PKR by InFusion cloning (Takara
609 Bio). PKR K296R and PKR T451A were obtained by InFusion mutagenesis (Takara Bio) on
610 pLenti MYC:PKR vector.

611 All primers used are listed in Appendix Table S1.

612

613 **Cell lines**

614 HEK293T, HEK293T/NoDice (2.20), HEK293T/NoDiceΔPKR cell lines were a gift from Pr.
615 Bryan Cullen (Duke University, Durham NC, USA) and described in (Bogerd *et al*, 2014;
616 Kennedy *et al*, 2015). Vero E6 cells were bought at ATCC (CRL-1586). Cell lines were tested
617 for Mycoplasma contamination.

618

619 **Cell culture and transfection**

620 Cells were maintained in Dulbecco's modified Eagle medium (DMEM, Gibco, Life
621 Technologies) supplemented with 10% fetal bovine serum (FBS, Clontech) in a humidified

622 atmosphere with 5% CO_2 at 37°C. Transfections were performed using Lipofectamine 2000
623 (Invitrogen, Fisher Scientific) according to the manufacturer's instructions.
624
625 **BAY 11-7082 treatment**
626 NoDice FHA:DICER WT and N1 cells were treated with BAY 11-7082 (Merck) by replacing
627 the culture medium with a medium containing the indicated BAY 11-7082 concentrations at
628 1µM or 5µM or the corresponding volume of DMSO only in the control conditions. Treatment
629 was maintained for 1h and media was changed with the infection media with SINV-GFP at an
630 MOI of 0.02 for 24h. Proteins, RNA and supernatants were then collected and analyzed.
631
632 **Lentivirus production and generation of stable cell lines**
633 The lentiviral supernatant from single transfer vector was produced by transfecting HEK293T
634 cells with 1.7µg of the transfer vector (either pLenti6 FHA-V5 or pLenti MYC), 0.33 µg of the
635 pVSV envelope plasmid (Addgene #8454) and 1.33µg of pSPAX2 packaging plasmid
636 (Addgene #12260) using Lipofectamine 2000 reagent (Invitrogen, Fisher Scientific) reagent
637 according to the manufacturer's protocol. HEK293T cells were maintained in DMEM (Gibco,
638 Life Technologies) medium supplemented with 10% Fetal bovine serum (FBS, Clontech). One
639 well from a 6-well-plate at 70% confluency was used for the transfection. The medium was
640 replaced 6 hours post-transfection. After 48 hours, the medium containing viral particles was
641 collected and filtered through a 0.45µm PES filter. Different cell lines were transduced: NoDice
642 (for N1, N1-CM, ΔHEL1, ΔHEL1-CM, ΔHEL2i, ΔHEL2i-CM, ΔHEL2 and ΔHEL2-CM),
643 NoDiceΔPKR (for WT, NA, ΔHEL1, ΔHEL1-CM, ΔHEL2i, ΔHEL2i-CM, ΔHEL2 and
644 ΔHEL2-CM), NoDiceΔPKR FHA:CTRL or FHA:DICER WT or FHA:DICER N1 (for CTRL,
645 PKR, K296R, T451A), NoDice or NoDiceΔPKR FHA DICER WT or N1 (for ACE2). One well
646 of a 6-well-plate was transduced using 500µL of filtered lentiviral supernatant either expressing

647 DICER or PKR or ACE2 constructs, 500µL of DMEM supplemented with 10% FBS and
648 4µg/mL polybrene (Merck, Sigma Aldrich) for 6 hours. Then, the medium was changed with
649 DMEM supplemented with 10% FBS for 24 hours and the resistant cell clones were selected
650 with the right antibiotic and subsequently maintained under the selection. For NoDice, the
651 selection lasted for 2 weeks with blasticidin at 15µg/mL (Invivogen). For NoDiceΔPKR, the
652 selection lasted for 2 weeks with blasticidin at 10µg/mL (Invivogen). For NoDiceΔPKR
653 FHA:CTRL or DICER WT, the selection lasted 11 days with hygromycin at 100µg/mL and for
654 NoDiceΔPKR FHA:DICER N1 it was the same but with hygromycin at 150µg/mL (Invivogen).
655 Lastly, the ACE2-tranduced cells were selected for 10 days with zeocin at 15µg/mL
656 (Invivogen).
657
658 **Viral stocks, virus infection**
659 Viral stocks of SINV WT, SINV-2A-GFP and SINV-GFP were produced as described in
660 (Girardi *et al*, 2015). SINV-2A-GFP was described in (Thomas *et al*, 2003). Cells were infected
661 with SINV (strain AR339), SINV-2A-GFP and SINV-GFP at an MOI of 0.02 and for SINV-
662 GFP at another MOI of 2 and samples were collected at the different indicated time points in a
663 BSL2 facility.
664 Viral stocks of SFV were propagated in Vero E6 cells from the initial stock (strain
665 UVE/SFV/UNK/XX1745; EVAg 001V-02468). Cells were infected at an MOI of 1.10^{-4} for 24
666 hours in a BSL2 facility.
667 Viral stocks of EV71 were produced by one passage in BHK21 cells from the initial stock
668 (ATCC VR-1432). Cells were infected at an MOI of 0.1 for 24 hours in a BSL2 facility.
669 Viral stocks of VSV-GFP were propagated in BHK21 cells from the initial stock (strain Indiana
670 isolate PI10; described in (Mueller *et al*, 2010)). Cells were infected at an MOI of 1.10^{-5} for 24
671 hours in a BSL2 facility.

672 Viral stocks of SARS-CoV-2 were produced by two passages in Vero E6 cells from the initial
673 stock (strain human/DEU/HH-1/2020; EVAg 002V-03991). Cells were infected at an MOI of
674 0.001 for 48 hours in a BSL3 facility.
675
676 **Analysis of viral titer by plaque assay**
677 For SINV, SINV-2A-GFP and SINV-GFP, Vero E6 cells were seeded in 96-well plates and
678 infected with 10-fold serial dilutions of infection supernatants for 1 hour. The inoculum was
679 removed and cells were covered with 2.5% carboxymethyl cellulose and cultured for 72 hours
680 at 37°C in a humidified atmosphere of 5% CO_2. Plaques were counted manually under the
681 microscope and viral titer was calculated according to the formula: *PFU/mL = #plaques/*
682 *(Dilution*Volume of inoculum).*
683 For SFV and VSV-GFP, Vero E6 cells were seeded in 24-well plates format and were infected
684 with 10-fold serial dilutions of infection supernatants for 1 hour. The inoculum was removed
685 and cells were covered with 2.5% carboxymethyl cellulose and cultured for 48 hours at 37°C
686 in a humidified atmosphere with 5% CO_2. For plaque visualization, the carboxymethyl cellulose
687 was removed. Cells were fixed with 4% formaldehyde (Merck, Sigma Aldrich) in PBS
688 (phosphate buffered saline, Gibco) for 20 minutes at room temperature (RT). Cells were then
689 stained with a 1X crystal violet solution for 20 minutes at RT (2% crystal violet, Sigma; 20%
690 ethanol; 4% formaldehyde, Merck). Plates were washed with clear water and plaques were
691 counted manually. The viral titer was calculated according to the formula: *PFU/mL = #plaques/*
692 *(Dilution*Volume of inoculum).*
693
694 **Analysis of viral titer by TCID50**
695 For EV71 and SARS-CoV-2, Vero E6 cells were seeded in 96-well plates already containing
696 10-fold serial dilutions of infection supernatants. Cells were maintained three to four days at

697 37°C in a humidified atmosphere with 5% CO_2. Wells containing dead cells were counted
698 manually under the microscope and viral titer was calculated according to the Spearman-
699 Kaerber 50% lethal dose formula described in (Wilham *et al*, 2010; Wulff *et al*, 2012).
700
701 **Live-cell imaging**
702 One-hundred thousand NoDice and NoDiceΔPKR polyclonal FHA:DICER WT, N1, ΔHEL1,
703 ΔHEL2i and ΔHEL2 cells were seeded in a 24-well plate and infected with SINV-GFP at an
704 MOI of 2. Uninfected cells were used as control. GFP fluorescence and phase contrast were
705 observed using a CellcyteX live-cell imaging system (Discover Echo). Six images per well
706 (10X objective) were acquired every 6 hour for 24 h and were analyzed with the Cellcyte Studio
707 software to determine cell confluency and GFP relative intensity.
708
709 **Western blot analysis**
710 Proteins were extracted and homogenized in the appropriate volume of ice-cold lysis buffer
711 (50mM Tris-HCl pH 7.5, 5mM EDTA, 150 mM NaCl, 0.05% SDS, 1% Triton X-100 and
712 protease inhibitor cocktail (complete Mini, Merck)). Proteins were quantified using the
713 Bradford method (Bio-Rad) and 30 µg of total protein extract were loaded on 10% acrylamide-
714 bis-acrylamide gels or 4-20% Mini-PROTEAN TGX Precast Gels (Bio-Rad). Proteins were
715 separated by migration at 135 V in 1X Tris-Glycine-SDS buffer (Euromedex). Proteins were
716 electro-transferred on a nitrocellulose membrane in 1X Tris-Glycine buffer supplemented with
717 20% ethanol. Equal loading was verified by Ponceau S staining (Merck). Membranes were
718 blocked for 1 hour at RT under stirring in 5% milk (Carl Roth) diluted in PBS-Tween (PBS-T)
719 0.2%. Membranes were probed with the following antibodies overnight at 4°C under stirring:
720 anti-hDICER (1:1000, A301-937A, Euromedex, Bethyl), anti-PKR (1:1000, ab32506 Abcam),
721 anti-PKR (1:1000, #12297 Cell signaling), anti-p-PKR (1:1000, ab 81303 Abcam), anti-PACT

722 (1:500, ab75749 Abcam), anti-TARBP2 (1:500, sc-514124, Cliniscience, Santa Cruz), anti-
723 HA-HRP (1:10000, 12013819001 Merck, Sigma Aldrich), anti-c-Myc (1:1000, ab32072
724 Abcam), anti-p-eIF2α (1:1000, #9721 Cell signaling), anti-α-Tubulin-HRP (1:10000, 1E4C11
725 Fisher Scientific), anti-SINV capsid (1:5000, kind gift from Dr. Diane Griffin, Johns Hopkins
726 University School of Medicine, Baltimore, MD), anti-GFP (1:1000, 11814460001 Merck,
727 Sigma Aldrich), anti-GAPDH-HRP (1:10000, G9545 Merck, Sigma Aldrich), anti-SARS-CoV-
728 2 Nucleocapsid (1:1000, ab273167 Abcam), anti-AGO2 (1:250, kind gift from Pr. Gunter
729 Meister, University of Regensburg), anti-ACE2 (1:1000, AF933 Bio-Techne), anti-NF-kB/p65
730 (1:1000, #8242 Cell signaling), anti-p-NF-kB/p65 (1:1000, #3033 Cell signaling) and anti-
731 IkBα (1:1000, #4812 Cell signaling). The detection was performed using a specific secondary
732 antibody coupled to the horseradish peroxidase (HRP): anti-mouse-HRP (1:4000, A4416
733 Merck, Sigma Aldrich), anti-rabbit-HRP (1:10000, #31460 Fisher Scientific), anti-rat-HRP
734 (1:10000, #31470 Fisher Scientific) and anti-goat-HRP (1:10000, #A15999 Invitrogen).
735 Detection was done using Chemiluminescent Substrate or SuperSignal West Femto maximum
736 sensitivity substrate (Pierce, Fisher Scientific) and visualized with a Fusion FX imaging system
737 (Vilber).
738 Panels IkBa (Appendix Figure-S4A), DICER (Figure 4B) and IkBa (Figure 8D) were contrasted
739 and adjusted uniformly using an image processing software. All the bands were quantified using
740 the FiJi software (Schindelin *et al*, 2012) and normalized to the housekeeping gene.
741
742 **RNA extraction**
743 Total RNA was extracted using TRI Reagent solution (Invitrogen, Fisher Scientific) according
744 to the manufacturer's instructions.
745
746 **Northern blot analysis**

747 5 micrograms of total RNA were loaded on a 17.5% acrylamide-urea 4 M gel and resolved in
748 1X Tris-Borate-EDTA buffer. Small RNAs were electro-transferred onto a nylon Hybond-NX
749 membrane (GE Healthcare) in 0.5X Tris-Borate-EDTA buffer. RNAs were chemically cross-
750 linked to the membrane for 90 minutes at 65°C using 1-ethyl-3-[3-
751 dimethylaminopropyl]carbodiimide hydrochloride (EDC) (Merck, Sigma Aldrich). The
752 membrane was pre-hybridized for 30 minutes in Perfect Hyb plus (Merck, Sigma Aldrich) at
753 50°C in rotation. Oligodeoxyribonucleotide probes (see Appendix Table S1) were labeled at
754 the 5'-end with 25 µCi of [γ-32P]dATP using T4 polynucleotide kinase (Fischer Scientific).
755 The unbound [γ-32P]dATP was removed with MicroSpin G-25 column (GE Healthcare) and
756 the probe was incubated overnight at 50°C with the membrane in rotation. The membrane was
757 washed twice with 5X SSC (Saline-Sodium citrate buffer, Euromedex), 0.1% SDS for 15
758 minutes at 50°C and once with 1X SSC (Euromedex), 0.1% SDS for 5 minutes at 50°C. The
759 membrane was exposed on a phosphorimaging plate in a cassette and the signal was recorded
760 using a Typhoon FLA-7000 laser scanner (GE Healthcare).
761
762 **RT-qPCR analysis**
763 DNaseI treatment was performed on 1µg of extracted RNAs (Invitrogen, Fisher Scientific).
764 DNase treated RNAs were then retro-transcribed using a random nonameric primer with the
765 SuperScript IV (SSIV) reverse transcriptase according to the manufacturer's instructions
766 (Invitrogen, Fisher Scientific). Real-time quantitative PCR was performed on 1/10 dilution of
767 cDNA using SYBR green PCR master mix (Fisher Scientific) and the primers listed in
768 Appendix Table S1.
769
770 **Strand-specific semi-quantitative RT-PCR on SINV antigenome**

771 Negative-strand-specific reverse transcription was performed using a primer specific to the 5'
772 region of the SINV plus-strand genome (nucleotides 1 to 42 – Appendix Table S1). 100 ng of
773 RNA, 1 µL of 2 µM specific primer, 1 µL of 10 mM dNTPs and water up to 13 µL final volume
774 were mixed and incubated at 65°C for 5 min. 4 µL of 5X SSIV Buffer (Invitrogen, Fisher
775 Scientific), 1 µL of 0.1M DTT (dithiothreitol), 1 µL of RNase inhibitor (Ribolock, Fisher
776 Scientific) and 1 µL of SSIV reverse transcriptase (Invitrogen) were added and the mix was
777 incubated at 55°C for 10 min then at 80°C for 10 min. 1/20 of the cDNA was amplified by PCR
778 using the GoTaq DNA polymerase mix (Promega) with specific antigenome primers (Appendix
779 Table S1). PCR products were loaded on a 1% agarose gel and gel pictures were taken with a
780 Fusion FX imaging system (Vilber).
781
782 **Immunoprecipitation**
783 Immunoprecipitations were done on tagged proteins. Cells were harvested, infected at the
784 corresponding MOI and time and washed once with ice-cold PBS (Gibco, Life Technologies)
785 and resuspended in 600µL of ice-cold lysis buffer (50 mM Tris-HCl pH 7.5, 140 mM NaCl, 1.5
786 mM $MgCl_2$, 0.1% NP-40 and protease inhibitor cocktail (complete Mini, Merck, Sigma
787 Aldrich). Cells were lysed for 10 min incubation on ice and lysates were cleared with a 15 min
788 centrifugation at 12000 g and 4°C. 25µL of the lysates were kept as protein INPUT. Then,
789 samples were divided in two and 40µL of magnetic beads coated with monoclonal anti-HA or
790 anti-MYC antibodies were added (MACS purification system, Miltenyi Biotech). The samples
791 were incubated for 1 hour at 4°C under rotation. Samples were sequentially loaded onto
792 µColumns (MACS purification system, Miltenyi Biotech). The columns were washed 4 times
793 with 200µL of lysis buffer. The elution was done with 95°C-pre-heated 2X Laemmli buffer
794 (20% glycerol, 4% SDS, 125mM Tris-HCl pH 6.8, 10% (v/v) 2-β-mercaptoethanol, 0.004%
795 Bromophenol Blue). Proteins were analyzed by western blot.

796

797 **Immunostaining**

798 Cells were plated on Millicell EZ 8-well slide (Merck Millipore) and infected with the different
799 viruses at the corresponding MOI and infection time. Then, cells were fixed for 10 minutes at
800 RT with 4% formaldehyde (Merck, Sigma Aldrich) diluted in PBS 1X (Gibco). Cells were
801 incubated with a blocking solution (5% normal goat serum, 0.1% Triton X-100, PBS 1X) for
802 1h at RT. Primary J2 antibody diluted in blocking solution was added at 1:1000 dilution for 3h
803 at RT. Cells were washed three times with PBS 1X-0.1% Triton X-100 (Phosphate buffered
804 saline- Triton, PBS-T) and incubated 1h at RT in the dark with a secondary antibody solution
805 containing goat anti-mouse Alexa 594 (A11032, Invitrogen, Fisher Scientific) fluorescent-
806 coupled antibody diluted to 1:1000 in PBS-T solution. After three washes with PBS-T, cell
807 nuclei were stained with DAPI diluted to 1:5000 in PBS 1X for 2 minutes at RT in the dark
808 (Life technologies, Fischer Scientific). Slides were finally mounted on coverslips and the
809 Fluoromount-G mounting media (Southern Biotech). Images were acquired using an
810 epifluorescence BX51 (Olympus) microscope with a mercury source illuminator (U-RFL-T,
811 Olympus) and with x40 immersion oil objective.

812

813 **Small RNA cloning and sequencing**

814 NoDice FHA:DICER WT or N1 cells were plated in P150mm petri dishes at 25000000 cells
815 per dish and infected the following day with SINV-GFP at an MOI of 0.02 for 24h. Cells were
816 collected in 1.3 mL of ice-cold lysis buffer (50 mM Tris-HCl pH 7.5, 150 mM NaCl, 5mM
817 EDTA, 1% NP-40, 0.5 mM DTT, 0.1 U/mL of RNase inhibitor and protease inhibitor cocktail
818 (complete Mini, Merck, Sigma Aldrich)). Cells were lysed by putting the extract on ice for 15
819 min. First, human AGO proteins were immunoprecipitated from whole extract to enrich for
820 loaded small-RNAs. AGO-IP was done following the protocol described in (Hauptmann *et al*,

821 2015). Briefly, 50 µL of magnetic Dynabeads coupled to G protein (Invitrogen, Fisher
822 Scientific) were coupled to anti-Flag M2 antibody (F1804, Merck, Sigma Aldrich) overnight at
823 4°C under rotation. The day after, Flag-TNRC6B WT or mutant (with Tryptophans mutated to
824 Alanines; called TNRC6B Ala) peptides were incubated with the coupled beads for 3 h at 4°C
825 under rotation. Meanwhile, lysates were cleared with a centrifugation step at 10000 g for 10min
826 at 4°C and 100 µL were kept as INPUT (20 µL for proteins and 80 µL for RNAs). Then, lysates
827 were divided in two and put on the beads coupled to the peptides and incubated at 4°C for 3h
828 under rotation. After 4 washing steps with 300 µL of ice-cold washing buffer, beads were split:
829 280 µL were eluted with 1mL of TRI Reagent solution (Invitrogen, Fisher Scientific) and RNAs
830 were isolated according to the manufacturer's instructions; 20 µL were kept for proteins
831 analysis of IP efficiency by western blot and 20µL of 95°C-pre-heated 2X Laemmli buffer were
832 added (20% glycerol, 4% SDS, 125mM Tris-HCl pH 6.8, 10% (v/v) 2-β-mercaptoethanol,
833 0.004% Bromophenol Blue).
834 Small RNA libraries were prepared using the Illumina TruSeq small RNA library preparation
835 kit according to the manufacturer's protocol (RS-200-0012, Illumina).
836 Samples were analyzed with a Bioanalyzer device, and only AGO-IPs with TNRC6B wild-type
837 peptide in infected conditions in triplicates were analyzed for both cell lines, while only one
838 AGO-IP TNRC6B Ala control was analyzed for each cell line.
839 Libraries were sequenced on an Illumina HiSeq 4000 sequencer as single-end 50 base reads at
840 the GenomEast platform at the Institute of Genetics and Molecular and Cellular Biology
841 (Illkirch, France). Image analysis and base calling were performed using RTA version 2.7.7
842 and bcl2fastq version 2.20.0.422.
843
844 **mRNA sequencing**

845 NoDice FHA:DICER WT or N1 cells were plated in P100mm petri dishes at 5000000 cells per
846 dish and infected the following day with SINV-GFP at an MOI of 2 for 12h or 0.02 for 24h.
847 Cells were collected in Trizol reagent (Invitrogen, Thermo Fisher Scientific) and RNAs were
848 isolated according to the manufacturer's instructions.
849 Library preparation and sequencing were performed at the GenomEast platform at the Institute
850 of Genetics and Molecular and Cellular Biology (Illkirch, France). RNA-Seq libraries were
851 generated according to the manufacturer's instructions from 250 ng of total RNA using the
852 Illumina Stranded mRNA Prep, Ligation kit (Reference Guide - PN 1000000124518) and IDT
853 for Illumina RNA UD Indexes Ligation (Illumina, San Diego, USA). Briefly, Oligo(dT)
854 magnetic beads were used to purify and capture the mRNA molecules containing polyA
855 tails.The purified mRNAs were then fragmented at 94°C for 2 min and copied into first strand
856 complementary DNA (cDNA) using reverse transcriptase and random primers. Second strand
857 cDNA synthesis further generated blunt-ended double-stranded cDNA and incorporated dUTP
858 in place of dTTP to achieve strand specificity by quenching the second strand during
859 amplification. Following A-tailing of DNA fragments and ligation of pre-index anchors, PCR
860 amplification was used to add indexes and primer sequences and to enrich DNA libraries (30
861 sec at 98°C; [10 sec at 98°C, 30 sec at 60°C, 30 sec at 72°C] x 12 cycles; 5 min at 72°C).
862 Surplus PCR primers were further removed by purification using SPRIselect beads (Beckman-
863 Coulter, Villepinte, France) and the final libraries were checked for quality and quantified using
864 capillary electrophoresis.
865 Libraries were sequenced on an Illumina HiSeq 4000 sequencer as paired-end 100 base reads.
866 Image analysis and base calling were performed using RTA version 2.7.7 and bcl2fastq version
867 2.20.0.422.
868
869 **Bioinformatics analysis of small RNA sequencing data**

870 Sequencing reads of sRNA-seq libraries were processed and analyzed with the following
871 workflow. Cutadapt v1.16 (Martin, 2011) was first run to trim the 3' adapter (command:
872 cutadapt -a TGGAATTCTCGGGTGCCAAGG -e 0.1 --no-indels -O 6 -m 18 --discard-
873 untrimmed -o <sample>-cutadapt.fastq <sample>.fastq) and an additional filter was applied to
874 only keep 18- to 32-nt long trimmed reads for further analyses. Sample quality checks were
875 performed before and after these preprocessing steps using FastQC v0.11.8
876 (https://www.bioinformatics.babraham.ac.uk/projects/fastqc/). Preprocessed reads were then
877 mapped simultaneously to the human (GENCODE Human (GRCh38.p13) release 41) and
878 SINV-GFP (private sequence derived from NC_001547.1 – RefSeq database) genomes, using
879 Bowtie v1.3.1 (Langmead *et al*, 2009) (command: bowtie -q --phred33-quals -v 2 -y -a --best -
880 -strata -m 30 -x hg38coreGencodeSINVGFP <sample>-preprocessed.fastq <sample>-
881 hg38coreGencodeSINVGFP.bwtmap). Only alignments from the lowest mismatch stratum
882 with at most 2 mismatches were reported for each read, provided that their number was not
883 exceeding 30.
884 For each library, small RNA reads deriving solely from SINV-GFP were computationally
885 extracted and further characterized. Representations of their length distribution and localization
886 along the viral genome were both made in R using a custom Shiny application based on the
887 ggplot2 (Wickham, 2009) and Bioconductor Gviz (Hahne & Ivanek, 2016) packages
888 respectively.
889 Furthermore, expressed human miRNAs (miRBase v22.1 (Kozomara & Griffiths-Jones, 2011),
890 among which known mirtrons (Wen *et al*, 2015), were also identified and quantified in each
891 library using BEDTools v2.30.0 (Quinlan & Hall, 2010) by comparing their genomic
892 coordinates to those of the original aligned reads and by counting only reads overlapping at
893 least 80% of the miRNAs sequence (command: bedtools intersect -a <sample>-
894 hg38coreGencodeSINVGFP.bwtmap.bed -b hsa-matmir.bed -f 0.80 -wa -wb -s). Multiple

895 mapped reads were weighted by the number of mapping sites in other miRNAs, and the final
896 counts obtained for each miRNA were rounded down before further analysis. Differential
897 miRNA expression analysis between the two AGO-IP conditions was then performed with the
898 DESeq2 package (Love *et al*, 2014) by using an adjusted p-value < 0.05 and an absolute log2
899 fold change > 1as thresholds to define statistical significance. The heatmap of the 50 most
900 abundant miRs expressed in the AGO-IP samples (regularized-logarithm (rlog) transformed
901 counts) and the MA plot of the DESeq2 results were made in R with the Heatmaply (Galili *et*
902 *al*, 2018) and ggplot2 (Wickham, 2009) packages respectively, inside the same custom Shiny
903 application as previously mentioned.
904
905 **Bioinformatics analysis of mRNA sequencing data**
906 RNA-seq data were processed and analyzed using the following workflow. The first 5'-end base
907 of each read, a T-overhang added during the library preparation with the Illumina Stranded
908 mRNA protocol, was first trimmed, before using Skewer v0.2.2 (Jiang *et al*, 2014) in paired-
909 end mode for average quality read filtering and adapter trimming (command: skewer -Q 25 -x
910 CTGTCTCTTATACACATCT -y CTGTCTCTTATACACATCT -l 31 -m pe -t 2 -o <sample>
911 --quiet <sample>_R1.fq <sample>_R2.fq). Sample quality checks were performed before and
912 after these preprocessing steps using FastQC v0.11.8
913 (https://www.bioinformatics.babraham.ac.uk/projects/fastqc/). Then, human full-length
914 protein-coding transcripts (GENCODE Human (GRCh38.p13) release 41) and SINV-GFP both
915 genomic and subgenomic transcripts (private sequence derived from NC_001547.1 – RefSeq
916 database) were quantified using Salmon v1.10.0 (Patro *et al*, 2017) in mapping-based mode
917 with the selective alignment algorithm and a decoy-aware transcriptome (command: salmon
918 quant -p 6 -i index/gencode41.hg38.sinv.decoys_index --libType A --seqBias --gcBias --
919 numBootstraps 30 -1 data/<sample>_preprocessed_R1.fq.gz -2

920 data/<sample>_preprocessed_R2.fq.gz -o salmon-quants/<sample>). Transcript-level
921 abundance and count estimates thus obtained were next imported into R and further analyzed
922 with the tximport (Soneson *et al*, 2015) and DESeq2 (Love *et al*, 2014) packages. Briefly,
923 original transcript-level counts were summarized to gene-level estimated counts and an offset
924 was produced from transcript-level abundance estimates to correct for changes to the average
925 transcript length across samples. Differential expression analyses between tested conditions
926 were then conducted at the gene-level, and statistical significance was defined with an adjusted
927 p-value < 0.05 and an absolute log2 fold change > 1 thresholds. Finally, gene set enrichment
928 analysis (GSEA) studies were performed using the GSEA_4.3.2 Mac application, as made
929 available by the Broad Institute and the University of California, San Diego (https://www.gsea-
930 msigdb.org/gsea/index.jsp) (Mootha *et al*, 2003; Subramanian *et al*, 2005). These analyses were
931 conducted on the DESeq2 normalized counts of each comparison dataset against the Hallmark
932 Gene Sets (v2023.1) provided by the Molecular Signatures Database (MSigDB) (Liberzon *et*
933 *al*, 2015), and by using the Human_Ensembl_Gene_ID_MSigDB.v2023.1.Hs.chip annotation
934 file and all other parameters by default, except the permutation type which was set to gene_set.
935 Heatmaps and volcano plots of RNA-seq differential expression data were generated in R using
936 respectively the pheatmap package and a custom Shiny application based on the ggplot2
937 (Wickham, 2009) and ggrepel (https://github.com/slowkow/ggrepel) packages, while the global
938 gene set enrichment dot plot was adapted from VisualizeRNAseq
939 (https://github.com/GryderArt/VisualizeRNAseq).
940

941 **Analysis of transcription factor enrichment**

942 Lists of NF-kB/p65, STAT1, STAT2, IRF2 and IRF3 regulated genes were downloaded from
943 Harmonizome (Rouillard *et al*, 2016). Genes from these lists that were differentially expressed
944 between the indicated RNAseq experimental conditions were selected, and their log2 fold

change was plotted as cumulative distribution histograms. The two-sample Kolmogorov-Smirnov test was used to assess whether each distribution was statistically different from the distribution of WT DICER cells infected with SINV vs. mock infected. p-values are indicated on each histogram.

Statistical analysis

All the plaque assay statistical analyes were done with PRISM 10 (GraphPad) using One-way or Two-way ANOVA with Sidak's or Dunnett's corrections with a p-value threshold at $p<0.05$ on the logarithmic values.

All the qPCR statistical analyses were done with PRISM 10 (GraphPad) using t-test with Welch's correction with a p-value threshold at $p<0.05$ on the log2 values or unpaired t-test on the log2 values.

Detailed statistical analysis for each figure can be found in the source data file "Statistics_details.xlxs".

Data availability

The datasets produced in this study have been deposited in NCBI's Gene Expression Omnibus (Edgar *et al*, 2002) and are accessible through GEO Series accession number GSE241798 (https://www.ncbi.nlm.nih.gov/geo/query/acc.cgi?acc=GSE241798).

ACKNOWLEDGEMENTS

We would like to thank members of the laboratory for fruitful discussions, as well as Pr. Petr Svoboda (Institute of Molecular Genetics of the Czech Academy of Sciences, Prague, Czech Republic) for sharing unpublished data and exchanging ideas, and the SCIGNE (Scientific Cloud Infrastructure in Grand Est) platform at the Hubert Curien Pluridisciplinary Institute

(IPHC, Strasbourg, France) as well as its computing team for providing the technical support, computing and storage facilities needed to analyze some of the sequencing data.

This work of the Interdisciplinary Thematic Institute IMCbio+, as part of the ITI 2021-2028 program of the University of Strasbourg, CNRS and Inserm, was supported by IdEx Unistra (ANR-10-IDEX-0002), by SFRI-STRAT'US project (ANR-20-SFRI-0012), EUR IMCBio (IMCBio ANR-17-EURE-0023) and Equipex Insectarium ANR-11-EQPX-0022 under the framework of the French Investments for the Future Program. It also benefited from an IdEx University of Strasbourg 2022 Attractivity grant. Sequencing was performed by the GenomEast platform, a member of the 'France Génomique' consortium (ANR-10-INBS-0009). MB was funded by a doctoral fellowship from the Ministère de l'enseignement supérieur, de la recherche et de l'innovation and from the Fondation pour la Recherche Médicale (grant number FDT202204014935). LG was funded by a postdoctoral fellowship from the Fondation pour la Recherche Médicale (funding number SPF202209015746). SP also received funding from the European Research Council (ERC-CoG-647455 RegulRNA).

DISCLOSURE AND COMPETING INTEREST STATEMENT

The authors declare that they have no conflict of interest.

988 **REFERENCES**

989 Ahmad S & Hur S (2015) Helicases in Antiviral Immunity: Dual Properties as Sensors and
990 Effectors. *Trends in Biochemical Sciences* 40: 576–585
991 Akhrymuk I, Frolov I & Frolova EI (2018) Sindbis Virus Infection Causes Cell Death by nsP2-
992 Induced Transcriptional Shutoff or by nsP3-Dependent Translational Shutoff. *J Virol* 92:
993 e01388-18
994 Backes S, Langlois RA, Schmid S, Varble A, Shim JV, Sachs D & tenOever BR (2014) The
995 Mammalian Response to Virus Infection Is Independent of Small RNA Silencing. *Cell*
996 *Reports* 8: 114–125
997 Baldaccini M & Pfeffer S (2021) Untangling the roles of RNA helicases in antiviral innate
998 immunity. *PLOS Pathogens* 17: e1010072
999 Bhargava A, Szachnowski U, Chazal M, Foretek D, Caval V, Aicher S-M, Pipoli Da Fonseca
1000 J, Jeannin P, Beauclair G, Monot M, *et al* (2023) Transcriptomic analysis of sorted lung
1001 cells revealed a proviral activity of the NF-κB pathway towards SARS-CoV-2. *iScience*:
1002 108449
1003 Bogerd HP, Whisnant AW, Kennedy EM, Flores O & Cullen BR (2014) Derivation and
1004 characterization of Dicer- and microRNA-deficient human cells. *RNA* 20: 923–937
1005 Bonnet MC, Weil R, Dam E, Hovanessian AG & Meurs EF (2000) PKR stimulates NF-kappaB
1006 irrespective of its kinase function by interacting with the IkappaB kinase complex. *Mol*
1007 *Cell Biol* 20: 4532–4542
1008 Christian F, Smith EL & Carmody RJ (2016) The Regulation of NF-κB Subunits by
1009 Phosphorylation. *Cells* 5: 12
1010 Chukwurah E & Patel RC (2018) Stress-induced TRBP phosphorylation enhances its
1011 interaction with PKR to regulate cellular survival. *Sci Rep* 8
1012 Daher A, Laraki G, Singh M, Melendez-Peña CE, Bannwarth S, Peters AHFM, Meurs EF,
1013 Braun RE, Patel RC & Gatignol A (2009) TRBP Control of PACT-Induced
1014 Phosphorylation of Protein Kinase R Is Reversed by Stress. *Molecular and Cellular*
1015 *Biology* 29: 254–265
1016 Deddouche S, Matt N, Budd A, Mueller S, Kemp C, Galiana-Arnoux D, Dostert C, Antoniewski
1017 C, Hoffmann JA & Imler J-L (2008) The DExD/H-box helicase Dicer-2 mediates the
1018 induction of antiviral activity in drosophila. *Nat Immunol* 9: 1425–1432
1019 Dey M, Cao C, Dar AC, Tamura T, Ozato K, Sicheri F & Dever TE (2005) Mechanistic Link
1020 between PKR Dimerization, Autophosphorylation, and eIF2α Substrate Recognition. *Cell*
1021 122: 901–913
1022 Donnelly N, Gorman AM, Gupta S & Samali A (2013) The eIF2α kinases: their structures and
1023 functions. *Cell Mol Life Sci* 70: 3493–3511
1024 Edgar R, Domrachev M & Lash AE (2002) Gene Expression Omnibus: NCBI gene expression
1025 and hybridization array data repository. *Nucleic Acids Res* 30: 207–210
1026 Farabaugh KT, Krokowski D, Guan B-J, Gao Z, Gao X-H, Wu J, Jobava R, Ray G, de Jesus
1027 TJ, Bianchi MG, *et al* (2020) PACT-mediated PKR activation acts as a hyperosmotic
1028 stress intensity sensor weakening osmoadaptation and enhancing inflammation. *eLife* 9:
1029 e52241
1030 Ferreira CB, Sumner RP, Rodriguez-Plata MT, Rasaiyaah J, Milne RS, Thrasher AJ, Qasim W

1031 & Towers GJ (2020) Lentiviral Vector Production Titer Is Not Limited in HEK293T by
1032 Induced Intracellular Innate Immunity. *Molecular Therapy - Methods & Clinical*
1033 *Development* 17: 209–219
1034 Flemr M, Malik R, Franke V, Nejepinska J, Sedlacek R, Vlahovicek K & Svoboda P (2013) A
1035 Retrotransposon-Driven Dicer Isoform Directs Endogenous Small Interfering RNA
1036 Production in Mouse Oocytes. *Cell* 155: 807–816
1037 Galili T, O'Callaghan A, Sidi J & Sievert C (2018) heatmaply: an R package for creating
1038 interactive cluster heatmaps for online publishing. *Bioinformatics* 34: 1600–1602
1039 Gibbings D, Mostowy S, Jay F, Schwab Y, Cossart P & Voinnet O (2012) Selective autophagy
1040 degrades DICER and AGO2 and regulates miRNA activity. *Nat Cell Biol* 14: 1314–1321
1041 Gil J, Rullas J, García MA, Alcamí J & Esteban M (2001) The catalytic activity of dsRNA-
1042 dependent protein kinase, PKR, is required for NF-κB activation. *Oncogene* 20: 385–394
1043 Girardi E, Chane-Woon-Ming B, Messmer M, Kaukinen P & Pfeffer S (2013) Identification of
1044 RNase L-dependent, 3'-end-modified, viral small RNAs in Sindbis virus-infected
1045 mammalian cells. *MBio* 4: e00698-00613
1046 Girardi E, Lefèvre M, Chane-Woon-Ming B, Paro S, Claydon B, Imler J-L, Meignin C &
1047 Pfeffer S (2015) Cross-species comparative analysis of Dicer proteins during Sindbis
1048 virus infection. *Sci Rep* 5: 10693
1049 Guo Z, Li Y & Ding S-W (2019) Small RNA-based antimicrobial immunity. *Nat Rev Immunol*
1050 19: 31–44
1051 Gurung C, Fendereski M, Sapkota K, Guo J, Huang F & Guo Y-L (2021) Dicer represses the
1052 interferon response and the double-stranded RNA-activated protein kinase pathway
1053 in mouse embryonic stem cells. *Journal of Biological Chemistry* 296: 100264
1054 Hahne F & Ivanek R (2016) Visualizing Genomic Data Using Gviz and Bioconductor. *Methods*
1055 *Mol Biol* 1418: 335–351
1056 Hauptmann J, Schraivogel D, Bruckmann A, Manickavel S, Jakob L, Eichner N, Pfaff J, Urban
1057 M, Sprunck S, Hafner M, *et al* (2015) Biochemical isolation of Argonaute protein
1058 complexes by Ago-APP. *Proc Natl Acad Sci U S A* 112: 11841–11845
1059 Hoffmann M, Kleine-Weber H, Schroeder S, Krüger N, Herrler T, Erichsen S, Schiergens TS,
1060 Herrler G, Wu N-H, Nitsche A, *et al* (2020) SARS-CoV-2 Cell Entry Depends on ACE2
1061 and TMPRSS2 and Is Blocked by a Clinically Proven Protease Inhibitor. *Cell* 181: 271-
1062 280.e8
1063 Ishii T, Kwon H, Hiscott J, Mosialos G & Koromilas AE (2001) Activation of the IκBα kinase
1064 (IKK) complex by double-stranded RNA-binding defective and catalytic inactive mutants
1065 of the interferon-inducible protein kinase PKR. *Oncogene* 20: 1900–1912
1066 Ito T, Yang M & May WS (1999) RAX, a Cellular Activator for Double-stranded RNA-
1067 dependent Protein Kinase during Stress Signaling *. *Journal of Biological Chemistry* 274:
1068 15427–15432
1069 Ivashkiv LB & Donlin LT (2014) Regulation of type I interferon responses. *Nature Reviews*
1070 *Immunology* 14: 36–49
1071 Jiang D, Guo H, Xu C, Chang J, Gu B, Wang L, Block TM & Guo J-T (2008) Identification of
1072 Three Interferon-Inducible Cellular Enzymes That Inhibit the Replication of Hepatitis C
1073 Virus. *Journal of Virology* 82: 1665–1678
1074 Jiang H, Lei R, Ding S-W & Zhu S (2014) Skewer: a fast and accurate adapter trimmer for

1075 next-generation sequencing paired-end reads. *BMC Bioinformatics* 15: 182
1076 Kanarek N & Ben-Neriah Y (2012) Regulation of NF-κB by ubiquitination and degradation of
1077 the IκBs. *Immunol Rev* 246: 77–94
1078 Kennedy EM, Whisnant AW, Kornepati AVR, Marshall JB, Bogerd HP & Cullen BR (2015)
1079 Production of functional small interfering RNAs by an amino-terminal deletion mutant
1080 of human Dicer. *Proc Natl Acad Sci U S A* 112: E6945-6954
1081 Kong J, Bie Y, Ji W, Xu J, Lyu B, Xiong X, Qiu Y & Zhou X (2023) Alphavirus infection
1082 triggers antiviral RNAi immunity in mammals. *Cell Rep* 42: 112441
1083 Kozomara A & Griffiths-Jones S (2011) miRBase: integrating microRNA annotation and deep-
1084 sequencing data. *Nucleic Acids Res* 39: D152-157
1085 Langmead B, Trapnell C, Pop M & Salzberg SL (2009) Ultrafast and memory-efficient
1086 alignment of short DNA sequences to the human genome. *Genome Biol* 10: R25
1087 Lehman CW, Smith A, Kelly J, Jacobs JL, Dinman JD & Kehn-Hall K (2022) EGR1
1088 Upregulation during Encephalitic Viral Infections Contributes to Inflammation and Cell
1089 Death. *Viruses* 14: 1210
1090 Liberzon A, Birger C, Thorvaldsdóttir H, Ghandi M, Mesirov JP & Tamayo P (2015) The
1091 Molecular Signatures Database (MSigDB) hallmark gene set collection. *Cell Syst* 1: 417–
1092 425
1093 Love MI, Huber W & Anders S (2014) Moderated estimation of fold change and dispersion for
1094 RNA-seq data with DESeq2. *Genome Biol* 15: 550
1095 Ma E, MacRae IJ, Kirsch JF & Doudna JA (2008) Autoinhibition of Human Dicer by Its
1096 Internal Helicase Domain. *Journal of Molecular Biology* 380: 237–243
1097 Maillard PV, Ciaudo C, Marchais A, Li Y, Jay F, Ding SW & Voinnet O (2013) Antiviral RNA
1098 interference in mammalian cells. *Science* 342: 235–238
1099 Maillard PV, Van der Veen AG, Deddouche-Grass S, Rogers NC, Merits A & Reis e Sousa C
1100 (2016) Inactivation of the type I interferon pathway reveals long double-stranded RNA-
1101 mediated RNA interference in mammalian cells. *EMBO J* 35: 2505–2518
1102 Manjunath L, Oh S, Ortega P, Bouin A, Bournique E, Sanchez A, Martensen PM, Auerbach
1103 AA, Becker JT, Seldin M, *et al* (2023) APOBEC3B drives PKR-mediated translation
1104 shutdown and protects stress granules in response to viral infection. *Nat Commun* 14: 820
1105 Martin M (2011) Cutadapt removes adapter sequences from high-throughput sequencing reads.
1106 *EMBnet.journal* 17: 10–12
1107 Meister G & Tuschl T (2004) Mechanisms of gene silencing by double-stranded RNA. *Nature*
1108 431: 343–9
1109 Montavon TC, Baldaccini M, Lefèvre M, Girardi E, Chane-Woon-Ming B, Messmer M,
1110 Hammann P, Chicher J & Pfeffer S (2021) Human DICER helicase domain recruits PKR
1111 and modulates its antiviral activity. *PLoS Pathog* 17: e1009549
1112 Mootha VK, Lindgren CM, Eriksson K-F, Subramanian A, Sihag S, Lehar J, Puigserver P,
1113 Carlsson E, Ridderstråle M, Laurila E, *et al* (2003) PGC-1alpha-responsive genes
1114 involved in oxidative phosphorylation are coordinately downregulated in human diabetes.
1115 *Nat Genet* 34: 267–273
1116 Mueller S, Gausson V, Vodovar N, Deddouche S, Troxler L, Perot J, Pfeffer S, Hoffmann JA,
1117 Saleh M-C & Imler J-L (2010) RNAi-mediated immunity provides strong protection
1118 against the negative-strand RNA vesicular stomatitis virus in Drosophila. *Proceedings of*

1119 *the National Academy of Sciences* 107: 19390–19395
1120 Nielsen CPS, Han L, Arribas-Hernández L, Karelina D, Petersen M & Brodersen P (2023)
1121 Sensing of viral RNA in plants via a DICER-LIKE Ribonuclease. 2023.01.10.523395
1122 doi:10.1101/2023.01.10.523395 [PREPRINT]
1123 Nilsson-Payant BE, Uhl S, Grimont A, Doane AS, Cohen P, Patel RS, Higgins CA, Acklin JA,
1124 Bram Y, Chandar V, *et al* (2021) The NF-κB Transcriptional Footprint Is Essential for
1125 SARS-CoV-2 Replication. *Journal of Virology* 95: 10.1128/jvi.01257-21
1126 Parameswaran P, Sklan E, Wilkins C, Burgon T, Samuel MA, Lu R, Ansel KM, Heissmeyer
1127 V, Einav S, Jackson W, *et al* (2010) Six RNA viruses and forty-one hosts: viral small
1128 RNAs and modulation of small RNA repertoires in vertebrate and invertebrate systems.
1129 *PLoS Pathog* 6: e1000764
1130 Patro R, Duggal G, Love MI, Irizarry RA & Kingsford C (2017) Salmon provides fast and bias-
1131 aware quantification of transcript expression. *Nat Methods* 14: 417–419
1132 Pichlmair A & Reis e Sousa C (2007) Innate recognition of viruses. *Immunity* 27: 370–383
1133 Pierce JW, Schoenleber R, Jesmok G, Best J, Moore SA, Collins T & Gerritsen ME (1997)
1134 Novel inhibitors of cytokine-induced IkappaBalpha phosphorylation and endothelial cell
1135 adhesion molecule expression show anti-inflammatory effects in vivo. *J Biol Chem* 272:
1136 21096–21103
1137 Poirier EZ, Buck MD, Chakravarty P, Carvalho J, Frederico B, Cardoso A, Healy L, Ulferts R,
1138 Beale R & Reis e Sousa C (2021) An isoform of Dicer protects mammalian stem cells
1139 against multiple RNA viruses. *Science* 373: 231–236
1140 Quinlan AR & Hall IM (2010) BEDTools: a flexible suite of utilities for comparing genomic
1141 features. *Bioinformatics* 26: 841–842
1142 Raven JF, Wang S, Kazemi S, Baltzis D, Hatzoglou M, Tremblay ML & Koromilas AE (2006)
1143 The eIF2α kinase PKR is a negative regulator of Stat1 and Stat3. *The FASEB Journal* 20:
1144 A496–A496
1145 Richardson SJ, Willcox A, Hilton DA, Tauriainen S, Hyoty H, Bone AJ, Foulis AK & Morgan
1146 NG (2010) Use of antisera directed against dsRNA to detect viral infections in formalin-
1147 fixed paraffin-embedded tissue. *J Clin Virol* 49: 180–185
1148 Rouillard AD, Gundersen GW, Fernandez NF, Wang Z, Monteiro CD, McDermott MG &
1149 Ma'ayan A (2016) The harmonizome: a collection of processed datasets gathered to serve
1150 and mine knowledge about genes and proteins. *Database* 2016: baw100
1151 Ryman KD, White LJ, Johnston RE & Klimstra WB (2002) Effects of PKR/RNase L-
1152 Dependent and Alternative Antiviral Pathways on Alphavirus Replication and
1153 Pathogenesis. *Viral Immunology* 15: 53–76
1154 Schindelin J, Arganda-Carreras I, Frise E, Kaynig V, Longair M, Pietzsch T, Preibisch S,
1155 Rueden C, Saalfeld S, Schmid B, *et al* (2012) Fiji: an open-source platform for biological-
1156 image analysis. *Nat Methods* 9: 676–682
1157 Seo GJ, Kincaid RP, Phanaksri T, Burke JM, Pare JM, Cox JE, Hsiang T-Y, Krug RM &
1158 Sullivan CS (2013) Reciprocal inhibition between intracellular antiviral signaling and the
1159 RNAi machinery in mammalian cells. *Cell Host Microbe* 14: 435–445
1160 Soneson C, Love MI & Robinson MD (2015) Differential analyses for RNA-seq: transcript-
1161 level estimates improve gene-level inferences. *F1000Res* 4: 1521
1162 Subramanian A, Tamayo P, Mootha VK, Mukherjee S, Ebert BL, Gillette MA, Paulovich A,

1163 Pomeroy SL, Golub TR, Lander ES, *et al* (2005) Gene set enrichment analysis: a
1164 knowledge-based approach for interpreting genome-wide expression profiles. *Proc Natl*
1165 *Acad Sci U S A* 102: 15545–15550
1166 Takahashi T, Nakano Y, Onomoto K, Murakami F, Komori C, Suzuki Y, Yoneyama M & Ui-
1167 Tei K (2018a) LGP2 virus sensor regulates gene expression network mediated by TRBP-
1168 bound microRNAs. *Nucleic Acids Res* 46: 9134–9147
1169 Takahashi T, Nakano Y, Onomoto K, Yoneyama M & Ui-Tei K (2018b) Virus Sensor RIG-I
1170 Represses RNA Interference by Interacting with TRBP through LGP2 in Mammalian
1171 Cells. *Genes (Basel)* 9
1172 Taylor DR, Tian B, Romano PR, Hinnebusch AG, Lai MMC & Mathews MB (2001) Hepatitis
1173 C Virus Envelope Protein E2 Does Not Inhibit PKR by Simple Competition with
1174 Autophosphorylation Sites in the RNA-Binding Domain. *Journal of Virology* 75: 1265–
1175 1273
1176 tenOever BR (2016) The Evolution of Antiviral Defense Systems. *Cell Host & Microbe* 19:
1177 142–149
1178 Thomas JM, Klimstra WB, Ryman KD & Heidner HW (2003) Sindbis virus vectors designed
1179 to express a foreign protein as a cleavable component of the viral structural polyprotein.
1180 *J Virol* 77: 5598–5606
1181 Tsai K, Courtney DG, Kennedy EM & Cullen BR (2018) Influenza A virus-derived siRNAs
1182 increase in the absence of NS1 yet fail to inhibit virus replication. *RNA*
1183 Uhl S, Jang C, Frere JJ, Jordan TX, Simon AE & tenOever BR (2023) ADAR1 Biology Can
1184 Hinder Effective Antiviral RNA Interference. *J Virol* 97: e0024523
1185 van der Veen AG, Maillard PV, Schmidt JM, Lee SA, Deddouche-Grass S, Borg A, Kjær S,
1186 Snijders AP & Reis e Sousa C (2018) The RIG-I-like receptor LGP2 inhibits Dicer-
1187 dependent processing of long double-stranded RNA and blocks RNA interference in
1188 mammalian cells. *EMBO J* 37
1189 Weber F, Wagner V, Rasmussen SB, Hartmann R & Paludan SR (2006) Double-Stranded RNA
1190 Is Produced by Positive-Strand RNA Viruses and DNA Viruses but Not in Detectable
1191 Amounts by Negative-Strand RNA Viruses. *J Virol* 80: 5059–5064
1192 Wen J, Ladewig E, Shenker S, Mohammed J & Lai EC (2015) Analysis of Nearly One
1193 Thousand Mammalian Mirtrons Reveals Novel Features of Dicer Substrates. *PLoS*
1194 *Comput Biol* 11: e1004441
1195 Wickham H (2009) ggplot2: Elegant Graphics for Data Analysis New York: Springer New
1196 York
1197 Wilham JM, Orrú CD, Bessen RA, Atarashi R, Sano K, Race B, Meade-White KD, Taubner
1198 LM, Timmes A & Caughey B (2010) Rapid End-Point Quantitation of Prion Seeding
1199 Activity with Sensitivity Comparable to Bioassays. *PLOS Pathogens* 6: e1001217
1200 Williams BR (1999) PKR; a sentinel kinase for cellular stress. *Oncogene* 18: 6112–6120
1201 Wulff NH, Tzatzaris M & Young PJ (2012) Monte Carlo simulation of the Spearman-Kaerber
1202 TCID50. *Journal of Clinical Bioinformatics* 2: 5
1203 Yeh JX, Park E, Schultz KLW & Griffin DE (2019) NF-κB Activation Promotes Alphavirus
1204 Replication in Mature Neurons. *Journal of Virology* 93: e01071-19
1205 Zapletal D, Taborska E, Pasulka J, Malik R, Kubicek K, Zanova M, Much C, Sebesta M,
1206 Buccheri V, Horvat F, *et al* (2022) Structural and functional basis of mammalian

1207 microRNA biogenesis by Dicer. *Molecular Cell* 82: 4064-4079.e13
1208 Zhang Y, Xu Y, Dai Y, Li Z, Wang J, Ye Z, Ren Y, Wang H, Li W, Lu J, *et al* (2021) Efficient
1209 Dicer processing of virus-derived double-stranded RNAs and its modulation by RIG-I-
1210 like receptor LGP2. *PLOS Pathogens* 17: e1009790
1211

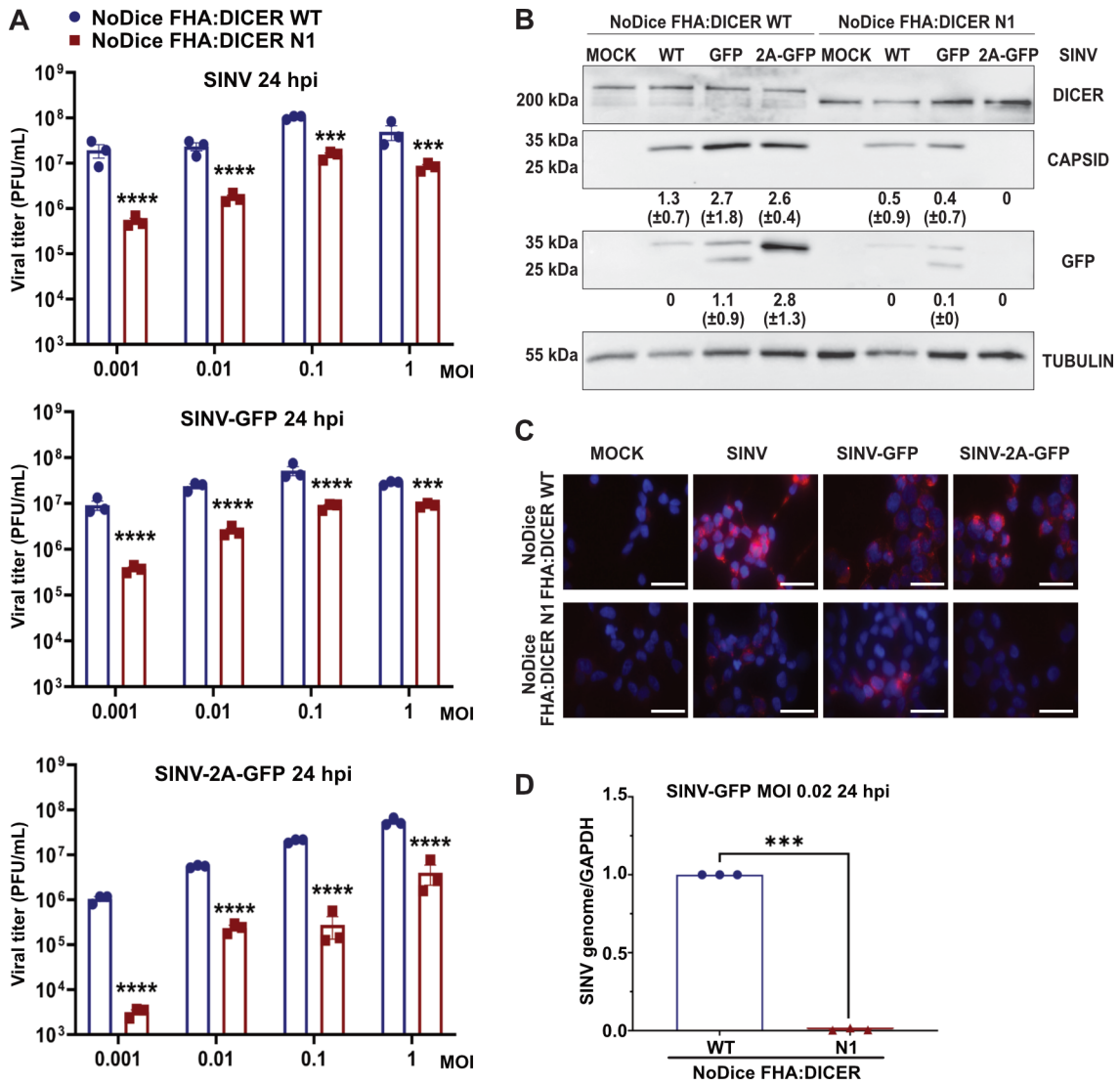

Figure 1. Dicer N1 decreases SINV viral accumulation in human cells
A. Mean (+/- SEM) of SINV, SINV-GFP and SINV-2A-GFP viral titers in NoDice FHA:DICER WT and N1 infected at an MOI ranging from 0.001 to 1 for 24h (n = 3 biological replicates) from plaque assay quantification. Ordinary two-way ANOVA test with Sidak's correction. ***: $p < 0.001$; ****: $p < 0.0001$. **B.** Western blot analysis of DICER, CAPSID and GFP expression in SINV, SINV-GFP and SINV-2A-GFP infected NoDice FHA:DICER WT and N1 cells at an MOI of 0.02 for 24h. Alpha-Tubulin was used as loading control. Band intensity was quantified and normalized to Tubulin for three independent biological replicates. Mean values (+/- SD) are indicated under the corresponding lane. **C.** Immunofluorescence analysis on NoDice FHA:DICER WT and N1 cells in mock, SINV, SINV-GFP and SINV-2A-GFP infected cells at an MOI of 0.02 for 24h. J2 antibody (red) was used to detect dsRNA upon infection. DAPI was used to stain the nuclei (blue). Scale bar = 100 µm, n = 3 biological replicates. **D.** RT-qPCR on SINV genome in NoDice FHA:DICER WT and N1 cells infected with SINV-GFP at an MOI of 0.02 for 24h. Mean (+/- SEM); n = 3 biological replicates. Unpaired t-test. ***: $p < 0.001$.

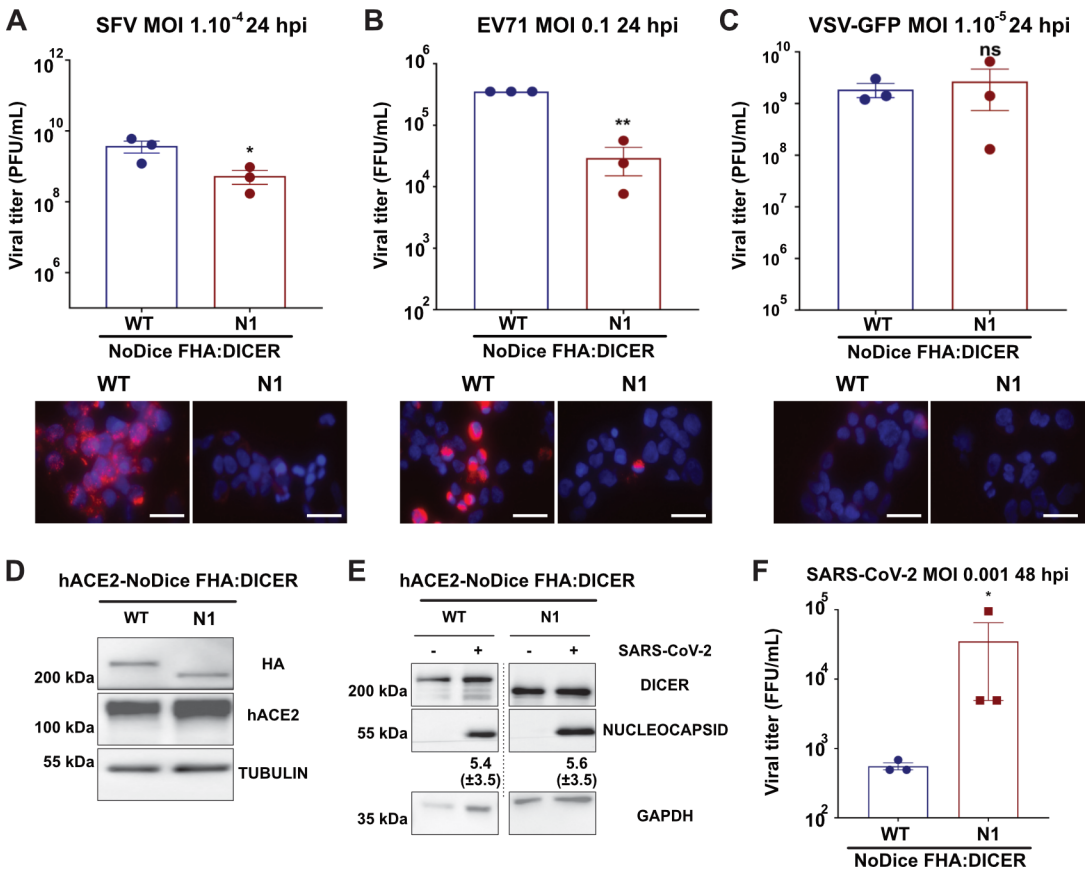

Figure 2. Dicer N1 is antiviral against alphaviruses and an enterovirus but not against a rhabdovirus and a coronavirus.

A. (Top) Mean (+/- SEM) of SFV viral titers in NoDice FHA:DICER WT and N1 cells infected at an MOI of 1.10^{-4} for 24h (n = 3 biological replicates) from plaque assay quantification. Unpaired t-test with Welch's correction. *: $p < 0.05$. (Bottom) Immunofluorescence analysis on NoDice FHA:DICER WT and N1 cells in SFV infected cells. J2 antibody (red) was used to detect dsRNA upon infection. DAPI was used to stain the nuclei (blue). Scale bar = 100 µm, n = 3 biological replicates. **B.** (Top) Mean (+/- SEM) of EV71 viral titers in NoDice FHA:DICER WT and N1 infected at an MOI of 0.1 for 24h (n = 3 biological replicates) from TCID50 quantification. Unpaired t-test. *: $p < 0.05$; **: $p<0.01$. (Bottom) Immunofluorescence analysis on NoDice FHA:DICER WT and N1 cells in EV71 infected cells. J2 antibody (red) was used to detect dsRNA upon infection. DAPI was used to stain the nuclei (blue). Scale bar = 100 µm, n = 3 biological replicates. **C.** (Top) Mean (+/- SEM) of VSV-GFP viral titers in NoDice FHA:DICER WT and N1 infected at an MOI of 1.10^{-5} for 24h (n = 3 biological replicates) from plaque assay quantification. Unpaired t-test. ns: non-significant. (Bottom) Immunofluorescence analysis on NoDice FHA:DICER WT and N1 cells in VSV-GFP infected cells. J2 antibody (red) was used to detect dsRNA upon infection. DAPI was used to stain the nuclei (blue). Scale bar = 100 µm, n = 3 biological replicates. **D.** Western blot analysis of human ACE2 and HA (for DICER) expression in NoDice FHA:DICER WT and N1 cells (n = 3 biological replicates). Alpha-Tubulin was used as loading control. **E.** Western blot analysis of DICER and NUCLEOCAPSID expression in SARS-CoV-2 infected NoDice FHA:DICER WT and N1 cells at an MOI of 0.001 for 48h. GAPDH was used as loading control. Band intensity was quantified and normalized to GAPDH for three independent biological replicates, then represented as mean (+/- SD) under the corresponding lane. **F.** Mean (+/- SEM) of SARS-CoV-2 viral titers in NoDice FHA:DICER WT and N1 infected at an MOI of 0.001 for 48h (n = 3 biological replicates) from TCID50 quantification. Unpaired t-test. *: $p < 0.05$.

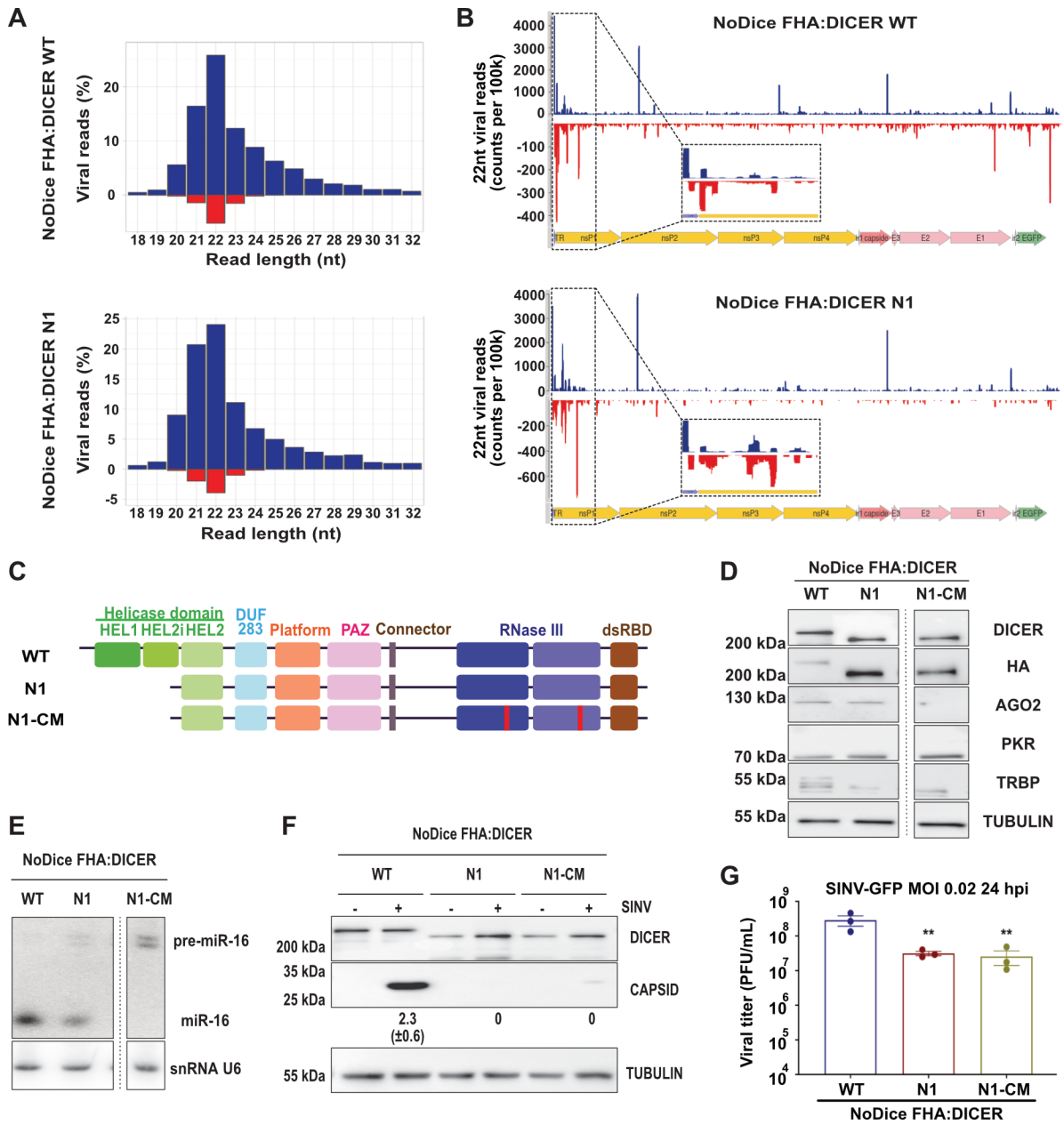

Figure 3. Dicer N1 catalytic activity is not involved in its antiviral phenotype
A. Representative histograms of the distribution of viral reads (in percent) per RNA length upon AGO proteins immunoprecipitation and small RNA sequencing in NoDice FHA:DICER WT (top) and N1 (bottom) cells infected with SINV-GFP at an MOI of 0.02 for 24h. Data from Replicate 1. Blue: positive strand; red: negative strand. **B.** Representative graphs of the mapping of 22-nt-reads on SINV-GFP genome in NoDice FHA:DICER WT (top) and N1 (bottom) cells. On the bottom: magnification of the mapping for the first 1000nt. Data from Replicate 1. Blue: positive strand; red: negative strand. **C.** Schematic representation of two Dicer mutants, N1 and N1-CM (catalytic mutant). In N1-CM, the two catalytic mutations are highlighted in red. **D.** Western blot analysis of DICER, HA, AGO2, PKR and TRBP expression in the monoclonal cell lines NoDice FHA:DICER WT, N1 and N1-CM (n = 3 biological replicates). Alpha-Tubulin was used as a loading control. **E.** Northern blot analysis of mirR-16 expression in the same samples as in D (n = 3 biological replicates). Expression of snRNA U6 was used as a loading control. **F.** Western blot analysis of DICER and CAPSID expression in SINV-GFP infected cells at an MOI of 0.02 for 24h. Alpha-Tubulin was used as loading control. Band

1274 intensity was quantified and normalized to Tubulin for three independent biological replicates,
1275 then represented as mean (+/- SD) under the corresponding lane. **G.** Mean (+/- SEM) of SINV-
1276 GFP viral titers in the same samples as in D, infected at an MOI of 0.02 for 24h (n = 3 biological
1277 replicates) from plaque assay quantification. Ordinary one-way ANOVA test with Dunnett's
1278 correction. **: $p < 0.01$.
1279

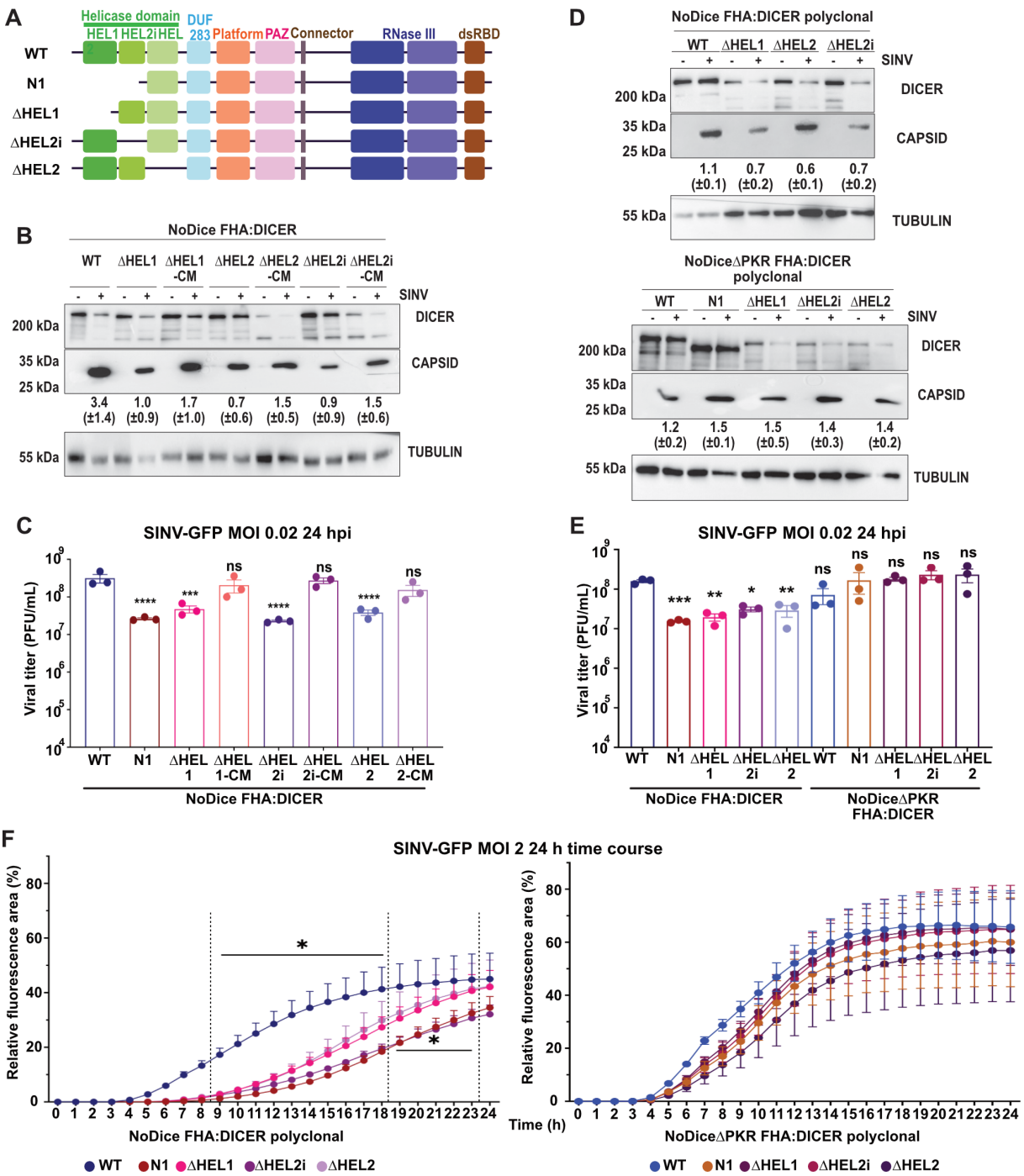

Figure 4. Dicer helicase sub-domains as well as PKR are important for Dicer antiviral activity

A. Schematic representation of the different Dicer helicase subdomain mutants. **B.** Western blot analysis of DICER and CAPSID expression in SINV-GFP infected cells at an MOI of 0.02 for 24h. Monoclonal NoDice FHA:DICER helicase mutant and their respective catalytic mutant cells are represented: WT, ΔHEL1, ΔHEL1-CM, ΔHEL2, ΔHEL2-CM, ΔHEL2i and ΔHEL2i-CM. Alpha-Tubulin was used as loading control. Band intensity was quantified and normalized to Tubulin for three independent biological replicates, then represented as mean (+/- SD) under the corresponding lane. **C.** Mean (+/- SEM) of SINV-GFP viral titers in the same samples as in B, infected at an MOI of 0.02 for 24h (n = 3 biological replicates) from plaque assay quantification. Ordinary one-way ANOVA test with Dunnett's correction. ***: $p < 0.001$; ****:

1293 $p < 0.0001$; ns: non-significant. **D.** Western blot analysis of DICER and CAPSID expression in
1294 SINV-GFP infected cells at an MOI of 0.02 for 24h. Polyclonal NoDice FHA:DICER (top) and
1295 NoDiceΔPKR FHA:DICER (bottom) helicase mutant cells are represented. Alpha-Tubulin was
1296 used as loading control. Band intensity was quantified and normalized to Tubulin for three
1297 independent biological replicates, then represented as mean (+/- SD) under the corresponding
1298 lane. **E.** Mean (+/- SEM) of SINV-GFP viral titers in the same samples as in D, infected at an
1299 MOI of 0.02 for 24h (n = 3 biological replicates) from plaque assay quantification. Ordinary
1300 one-way ANOVA test with Dunnett's correction. *: $p < 0.05$; **: $p < 0.01$; ***: $p < 0.001$; ns:
1301 non-significant. **F.** Mean (+/- SEM) of SINV-GFP fluorescence detection per cell area in the
1302 same samples as in D and E, infected at an MOI of 2 between 0 and 24h (n = 3 biological
1303 replicates). In NoDice cells, all differences were significant (*: $p < 0.05$) between 9 and 18hpi,
1304 but were only significant for Dicer N1 and ΔHEL2i-expressing cells between 19 and 23 hpi. At
1305 earlier time points, significance was not reached. In NoDiceΔPKR cells, significance was never
1306 reached. Ordinary two-way ANOVA test with Dunnett's correction.
1307
1308

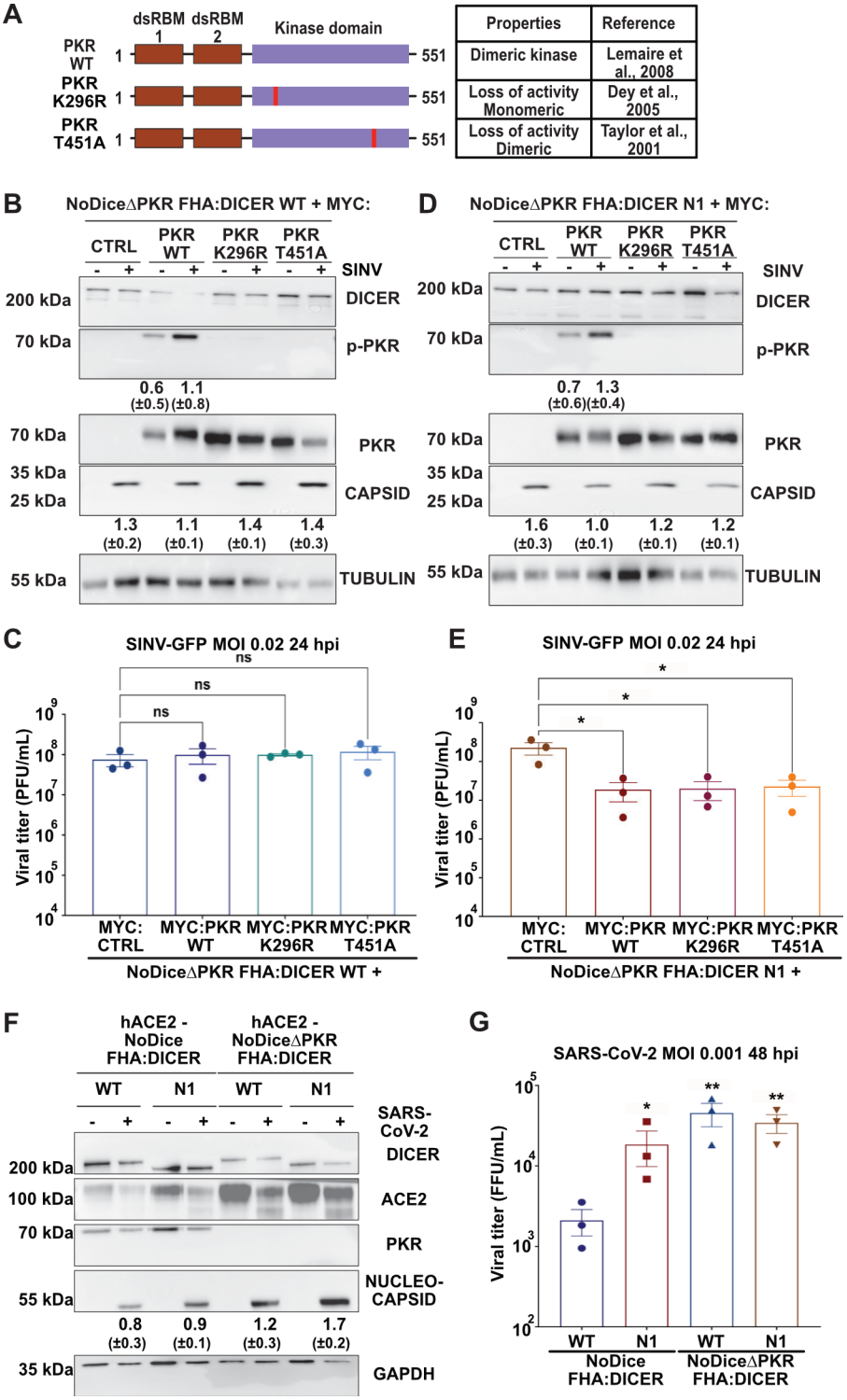

Figure 5. PKR requirements for Dicer N1 anti- or pro-viral activity

A. Schematic representation of PKR and its two point mutants: K296R and T451A. **B.** Western blot analysis of DICER, p-PKR, PKR and CAPSID expression in SINV-GFP infected NoDiceΔPKR FHA:DICER WT cells expressing MYC:EMPTY CTRL vector, MYC:PKR, MYC K296R or MYC:T451A at an MOI of 0.02 for 24h. Alpha-Tubulin was used as loading control. Band intensity was quantified and normalized to Tubulin for three independent biological replicates, then represented as mean (+/- SD) under the corresponding lane; p-PKR = p-PKR/PKR quantification. **C.** Mean (+/- SEM) of SINV-GFP viral titers in the same samples as in B, infected at an MOI of 0.02 for 24h (n = 3 biological replicates) from plaque assay

1320 quantification. Ordinary one-way ANOVA test with Dunnett's correction. ns: non-significant.
1321 **D.** Western blot analysis of DICER, p-PKR, PKR and CAPSID expression in SINV-GFP
1322 infected NoDiceΔPKR FHA:DICER N1 cells expressing MYC:EMPTY CTRL vector,
1323 MYC:PKR, MYC K296R or MYC:T451A at an MOI of 0.02 for 24h. Alpha-Tubulin was used
1324 as loading control. Band intensity was quantified and normalized to Tubulin for three
1325 independent biological replicates, then represented as mean (+/- SD) under the corresponding
1326 lane; p-PKR = p-PKR/PKR quantification. **E.** Mean (+/- SEM) of SINV-GFP viral titers in the
1327 same samples as in D, infected at an MOI of 0.02 for 24h (n = 3 biological replicates) from
1328 plaque assay quantification. Ordinary one-way ANOVA test with Dunnett's correction. *: $p <$
1329 0.05. **F.** Western blot analysis of DICER, human ACE2, PKR and NUCLEOCAPSID
1330 expression in SARS-CoV-2 infected NoDice FHA:DICER WT or N1 and NoDiceΔPKR
1331 FHA:DICER WT or N1 cells at an MOI of 0.001 for 48h. GAPDH was used as loading control.
1332 Band intensity was quantified and normalized to GAPDH for three independent biological
1333 replicates, then represented as mean (+/- SD) under the corresponding lane. **G.** Mean (+/- SEM)
1334 of SARS-CoV-2 viral titers in the same samples as in F, infected at an MOI of 0.001 for 48h (n
1335 = 3 biological replicates) from TCID50 quantification. Unpaired t-test with Welch's correction.
1336 *: $p < 0.05$; **: $p<0.01$.
1337
1338

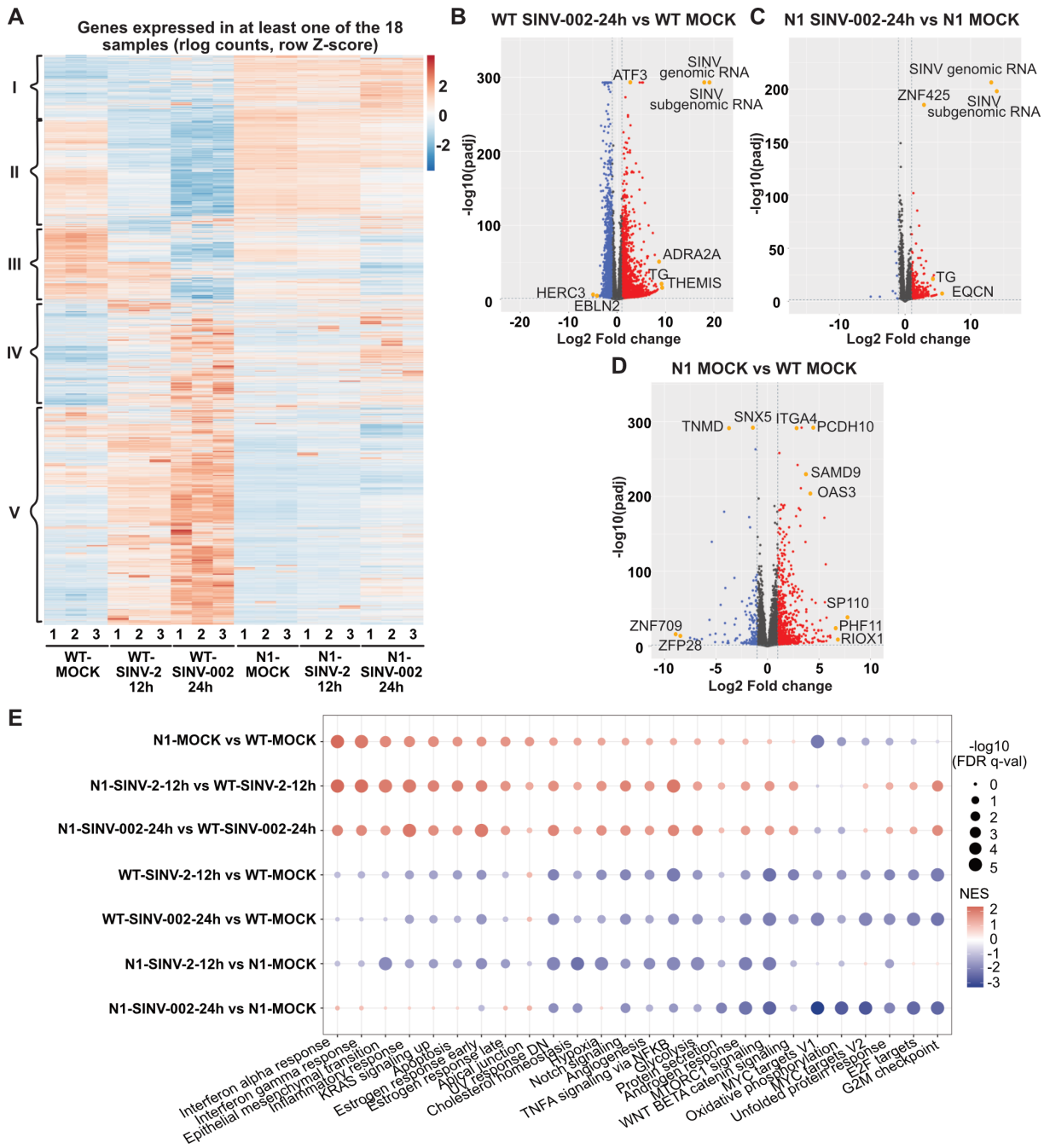

Figure 6. Dicer N1 and WT cells exhibit transcriptomic differences linked to an immune-related response

A. Z-score hierarchical clustering heatmap of genes identified by RNA sequencing analysis as differentially expressed between WT vs. N1 cells, either mock or SINV-infected cells (MOI 2 12 hpi or MOI 0.02 24 hpi). Gene clusters are delimited with black brackets and numbered from I to V. **B-D.** Volcano plots for differentially expressed genes (DEGs) between SINV-infected (MOI of 0.02 for 24h) and mock NoDice FHA:DICER WT cells (B); SINV-infected and mock NoDice FHA:DICER N1 cells (C); mock NoDice FHA:DICER WT and mock NoDice FHA:DICER N1 cells (D). Each gene is marked as a dot (red: upregulated ≥ 2-fold, blue: downregulated ≤ 2-fold, grey: unchanged). The horizontal line denotes an adjusted p-value of 0.05 (Wald test, DESeq2 package) and the vertical ones the Log2 fold change cut-off (-1 and 1). (n = 3 biological replicates). **E.** Biological states and processes associated terms enrichment performed with GSEA using the hallmark gene sets. Colors indicate NES (normalized

enrichment score) that are either positive (red) or negative (blue). Dot size corresponds to -log10(FDR q-val) of enrichment.

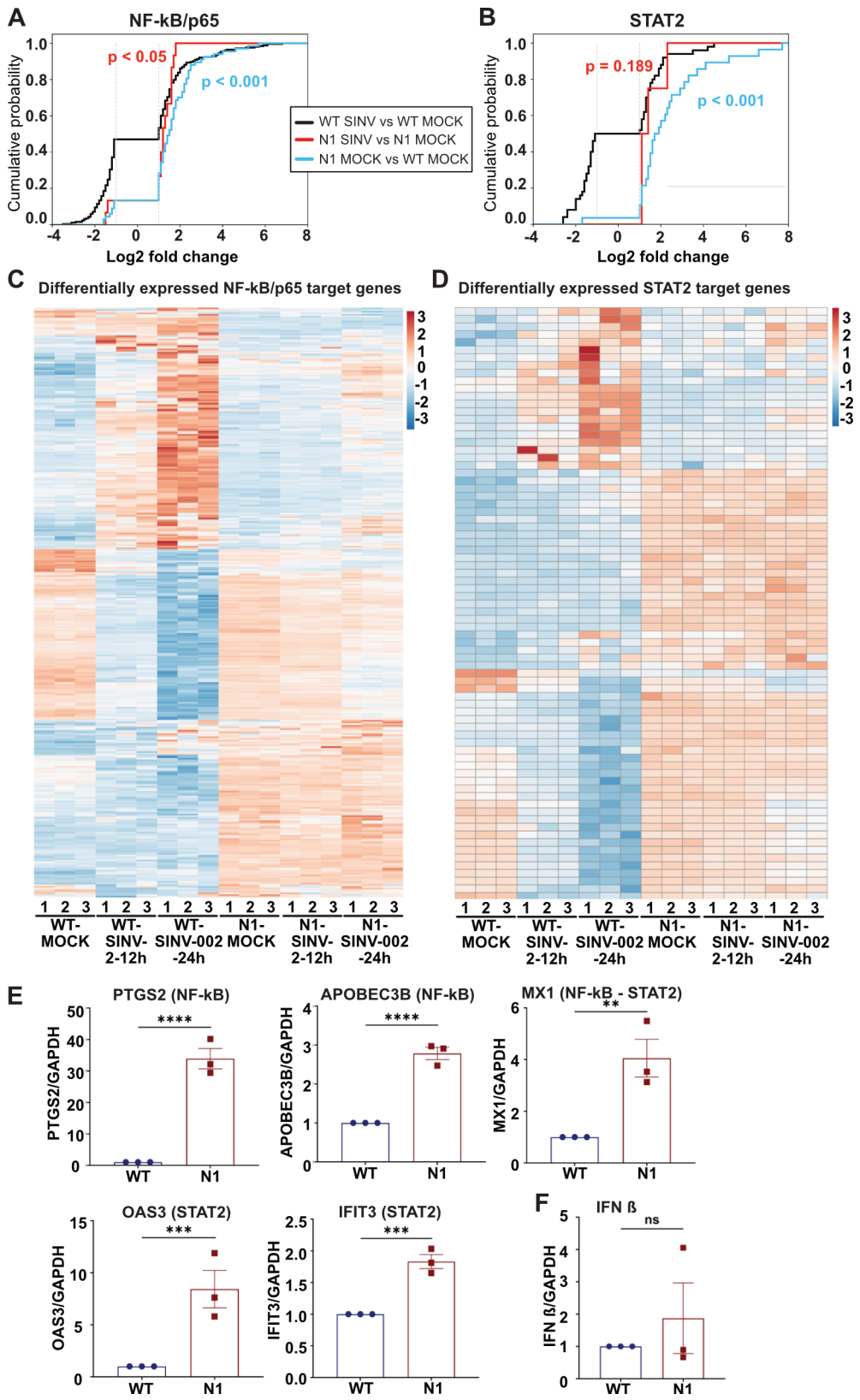

Figure 7. NF-kB/p65 and STAT2 transcription factors are involved in Dicer N1 cells transcriptomic changes

A-B. Histograms representing the cumulative probability of differentially expressed genes controlled by the transcription factors NF-kB/p65 (A) or STAT2 (B), plotted according to their Log2 fold change. The vertical lines stand for the Log2 fold change cut-off (-1 and 1). The two-

sample Kolmogorov-Smirnov test was used to assess whether each distribution was statistically different from the distribution of NoDice FHA:DICER WT cells infected with SINV vs. mock. p-values are indicated on each histogram. Black: WT SINV-002-24h vs WT MOCK; red: N1 SINV-002-24h vs N1 MOCK; blue: N1 MOCK vs WT MOCK. **C-D.** Z-score hierarchical clustering heatmap of genes identified by RNA sequencing analysis as differentially expressed between WT vs. N1 cells, either mock or SINV-infected cells (MOI 2 12 hpi or MOI 0.02 24 hpi). Each heatmap represents differentially expressed genes controlled by one transcription factor: NF-kB/p65 (C) or STAT2 (D). **E.** RT-qPCR on upregulated genes in the N1 MOCK vs WT MOCK condition and controlled by either NF-kB/p65 or STAT2. Mean (+/- SEM); n = 3 biological replicates. Unpaired t-test. **: $p < 0.01$; ***: $p < 0.001$; ****: $p < 0.0001$. **F.** RT-qPCR on IFN ß gene in WT and N1 cells in mock condition. Mean (+/- SEM); n = 3 biological replicates. Unpaired t-test. ns: non-significant.

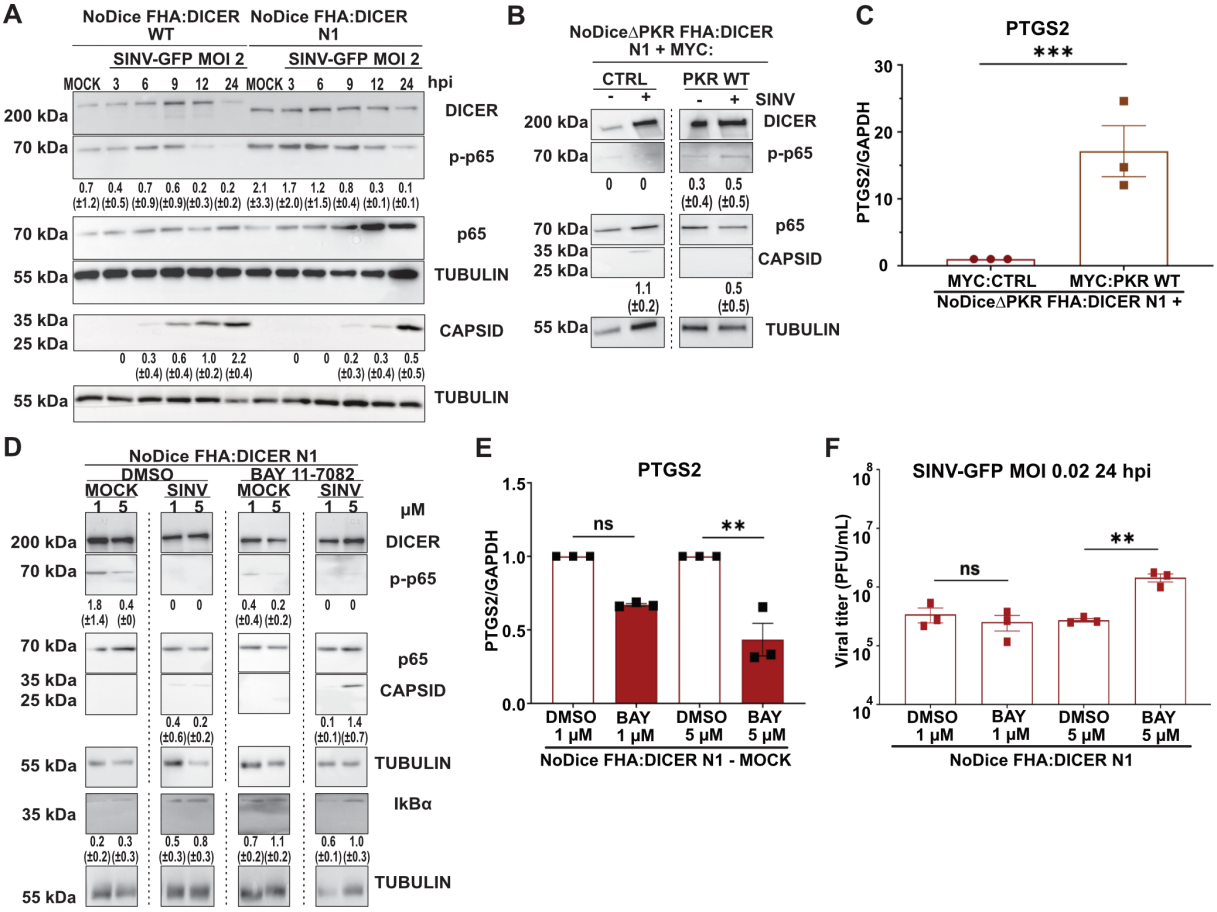

Figure 8. NF-kB/p65 is activated by PKR in Dicer N1 cells and is involved in their antiviral phenotype

A. Western blot analysis of DICER, p-p65, p65 and CAPSID expression in SINV-GFP infected NoDice FHA:DICER WT and N1 cells at an MOI of 0.02 between 3 and 24h. Alpha-Tubulin was used as loading control. Band intensity was quantified and normalized to Tubulin for three independent biological replicates, then represented as mean (+/- SD) under the corresponding lane; p-p65 = p-p65/p65 quantification. **B.** Western blot analysis of DICER, p-p65, p65 and CAPSID in SINV-GFP infected NoDiceΔPKR FHA:DICER N1 cells expressing MYC:EMPTY CTRL vector or MYC:PKR at an MOI of 0.02 for 24h. Alpha-Tubulin was used as loading control. Band intensity was quantified and normalized to Tubulin for three independent biological replicates, then represented as mean (+/- SD) under the corresponding lane; p-p65 = p-p65/p65 quantification. **C.** RT-qPCR on PTGS2 (NF-kB/p65 target) in the same samples as in B, in mock condition only. Mean (+/- SEM), n = 3 biological replicates. Unpaired t-test. ***: $p < 0.001$. **D.** Western blot analysis of DICER, p-p65, p65, CAPSID and IkBα expression in SINV-GFP infected NoDice FHA:DICER N1 cells at an MOI of 0.02 for 24h. Before infection, cells were treated with the NF-kB/p65 inhibitor, BAY 11-7082 or the vehicle (DMSO) at the indicated concentrations for 1 h. Alpha-Tubulin was used as loading control. Band intensity was quantified and normalized to Tubulin for three independent biological replicates, then represented as mean (+/- SD) under the corresponding lane; p-p65 = p-p65/p65 quantification. **E.** RT-qPCR on PTGS2 (NF-kB/p65 target) in NoDice FHA:DICER N1 mock cells treated with BAY 11-7082 or the vehicle (DMSO) at the indicated concentrations for 1h. Mean (+/- SEM), n = 3 biological replicates. Ordinary one-way ANOVA with Sidak's correction. **: $p < 0.01$; ns: non-significant. **F.** Mean (+/- SEM) of SINV-GFP viral titers in the same samples as in D, infected at an MOI of 0.02 for 24h (n = 3 biological replicates) from

1405 plaque assay quantification. Ordinary one-way ANOVA test with Sidak's correction. **: $p <$
1406 0.01; ns: non-significant.
1407
1408

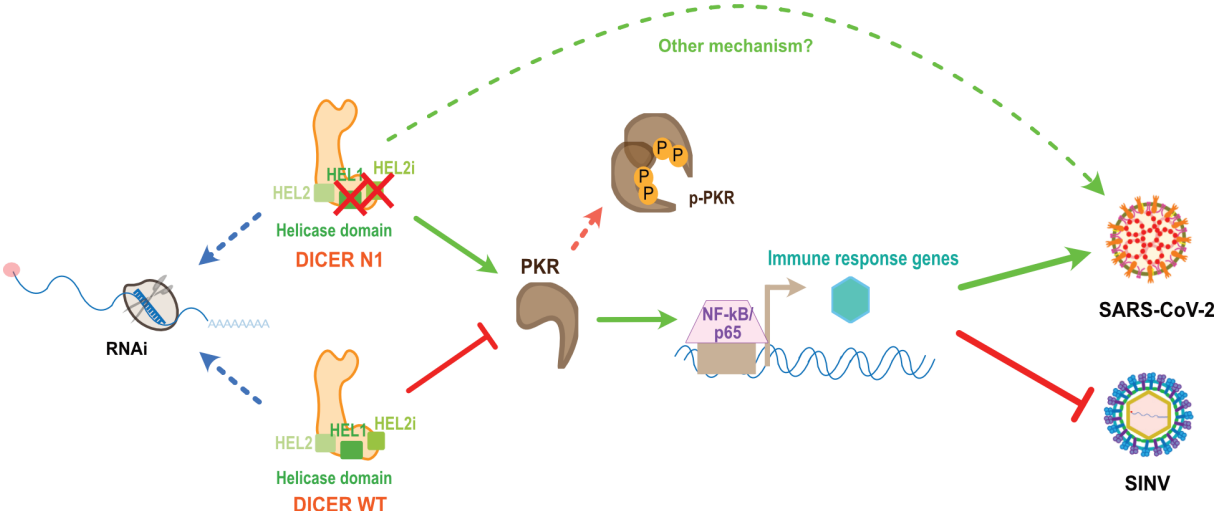

Figure 9. The Dicer N1 antiviral property is primed by PKR activation of NF-kB/p65 in mock cells.

With the first two parts of its helicase domain deleted, Dicer N1 is antiviral against SINV but pro-viral for SARS-CoV-2. This phenotype does not depend on RNAi, but instead relies on the presence of PKR in N1 cells. Nonetheless, PKR catalytic and/or dimerization activities are not required in that case. PKR is needed to activate a basal transcriptional response in Dicer N1 cells relying on immune-related transcription factors such as NF-kB/p65. NF-kB/p65 is directly involved in Dicer N1 antiviral phenotype thanks to its priming in Dicer N1 mock cells. However, we cannot exclude the existence of another mechanism that may favor SARS-CoV-2 infection.

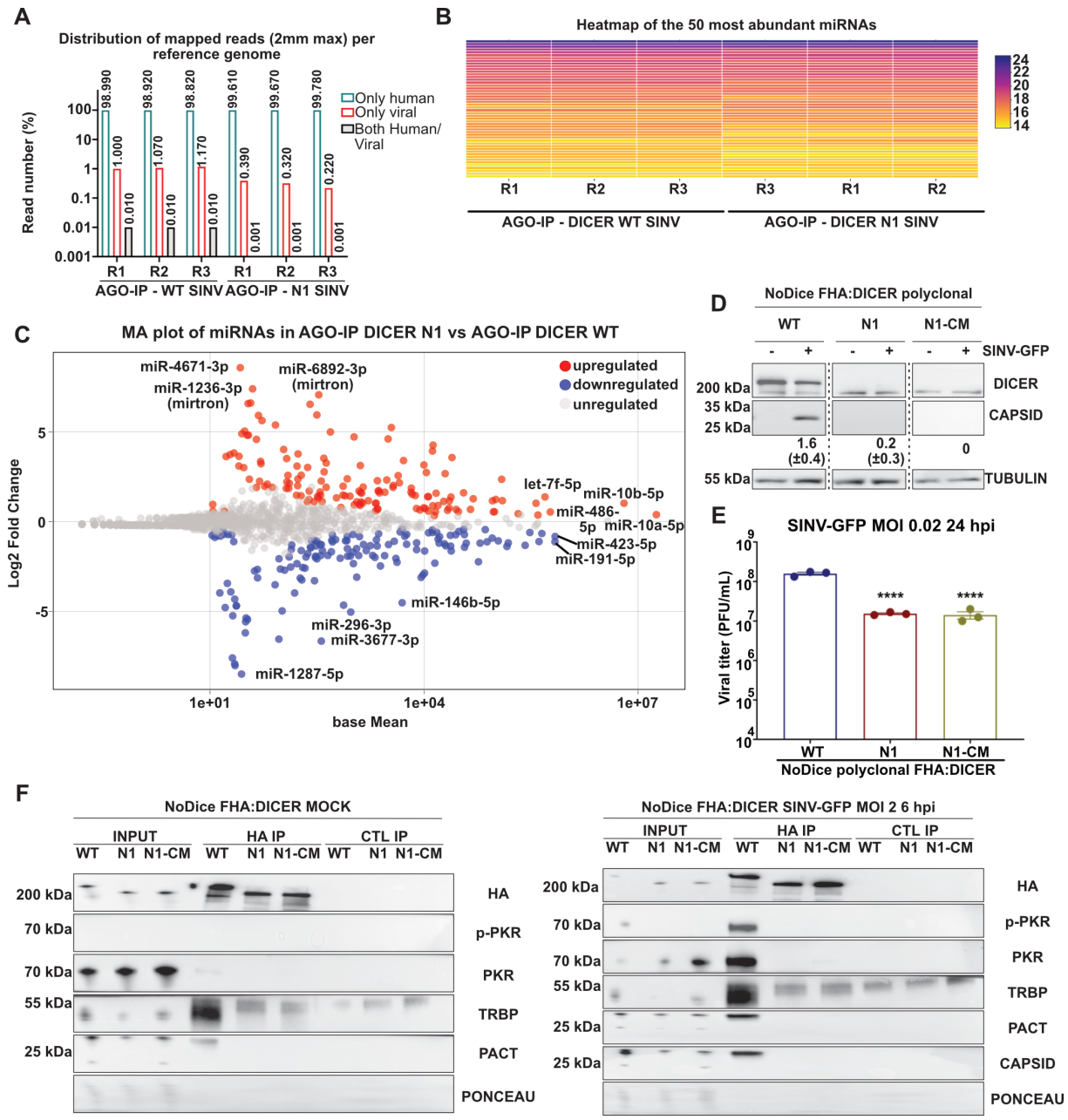

Figure EV1. Dicer N1 retains the same miRNA profile and interacting partners upon infection

A. Representation of small RNA reads distribution (in percent) upon AGO-IP in the three replicates for NoDice FHA:DICER WT and N1. Green: reads mapping to human RNAs only; Red: reads mapping to viral RNAs only; grey: reads mapping to both human and viral RNAs. **B.** Heatmap representing the relative expression levels of the 50 most abundant human miRNAs in all three replicates upon AGO-IP followed by small RNA sequencing in SINV-GFP infected NoDice FHA:DICER WT and N1 cells at an MOI of 0.02 for 24h. **C.** MA plot for miRNA enrichment upon AGO-IP followed by small RNA sequencing in SINV-GFP infected NoDice FHA:DICER N1 vs WT cells at an MOI of 0.02 for 24h. Each dot represents a miRNA either up- (red), down- (blue) or un-regulated (grey). **D,** Western blot analysis of DICER and CAPSID expression in SINV-GFP infected polyclonal NoDice FHA:DICER WT, N1 and N1-CM cells at an MOI of 0.02 for 24h. Alpha-Tubulin was used as loading control. Band intensity was quantified and normalized to Tubulin for three independent biological replicates, then represented as mean (+/- SD) under the corresponding lane. **E.** Mean (+/- SEM) of SINV-GFP

1440 viral titers in the same samples as in D, infected at an MOI of 0.02 for 24h (n = 3 biological
1441 replicates) from plaque assay quantification. Ordinary one-way ANOVA test with Dunnett's
1442 correction. ****: $p < 0.0001$. **F.** Western blot analysis of Dicer interacting partners upon HA-
1443 IP in NoDice FHA:DICER WT, N1 and N1-CM cells, in mock (left) or SINV-GFP infected
1444 (right) conditions at an MOI of 2 for 6h (n = 3 biological replicates). Anti-HA antibodies were
1445 used to validate the immunoprecipitation and Ponceau was used as a loading control.
1446
1447

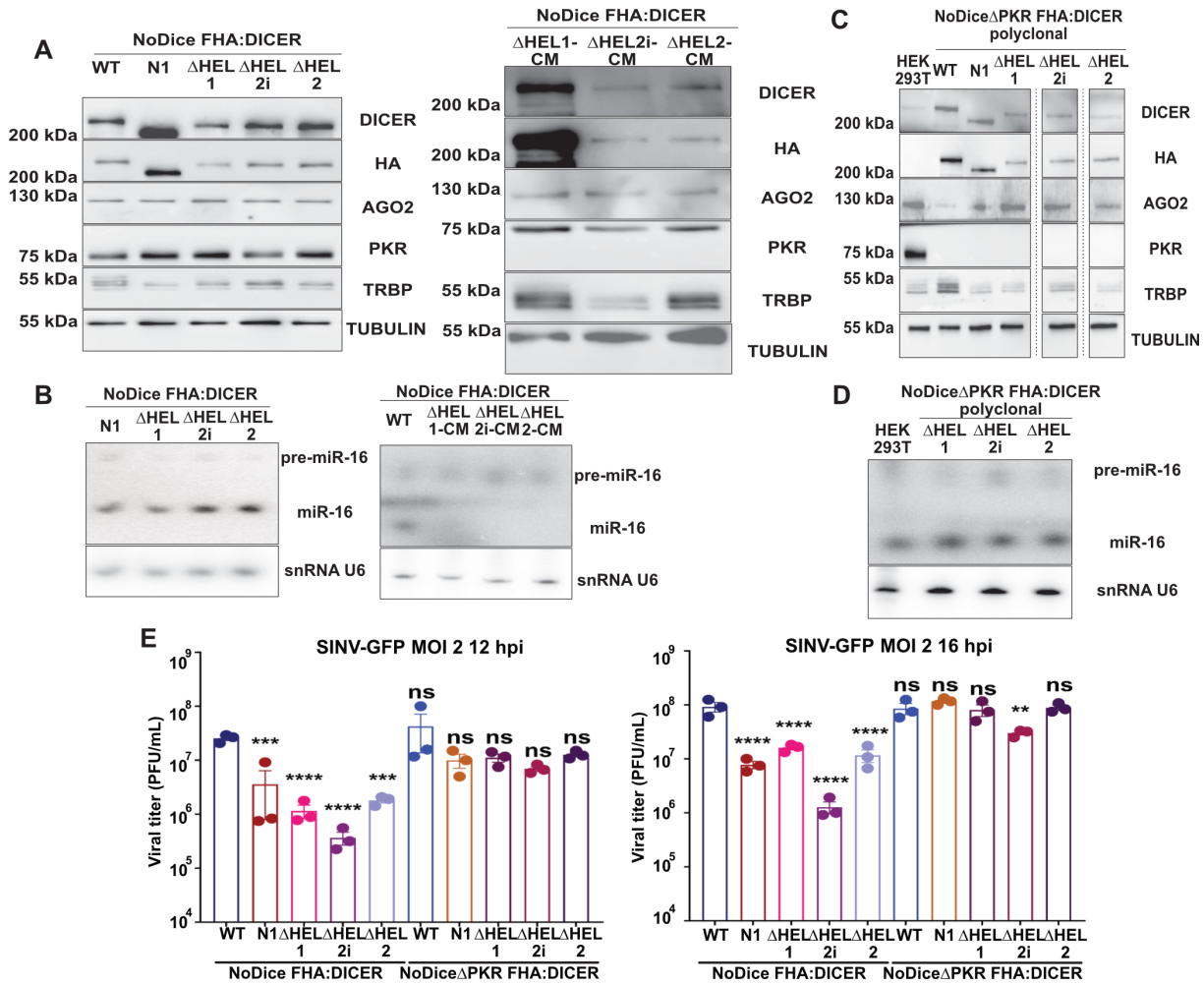

Figure EV2. The helicase sub-domains as well as PKR are important for Dicer antiviral activity

A. Western blot analysis of DICER, HA, AGO2, PKR and TRBP expression in the monoclonal cell lines NoDice FHA:DICER WT, N1, ΔHEL1, ΔHEL2i and ΔHEL2 (left, n = 3 biological replicates) and ΔHEL1-CM, ΔHEL2i-CM and ΔHEL2-CM (right, n = 2 biological replicates). Alpha-Tubulin was used as a loading control. **B.** Northern blot analysis of mirR-16 expression in the same samples as in A (n = 3 biological replicates for ΔHEL1, 2i and 2; n = 2 biological replicates for ΔHEL1-CM, 2i-CM and 2-CM). Expression of snRNA U6 was used as a loading control. **C.** Western blot analysis of DICER, HA, AGO2, PKR and TRBP expression in the polyclonal cell lines NoDiceΔPKR FHA:DICER WT, N1, ΔHEL1, ΔHEL2i and ΔHEL2 (n = 1 biological replicate). Alpha-Tubulin was used as a loading control. **D,** Northern blot analysis of mirR-16 expression in the same samples as in C (n = 2 biological replicates). Expression of snRNA U6 was used as a loading control. **E.** Mean (+/- SEM) of SINV-GFP viral titers in the polyclonal cell lines NoDice and NoDiceΔPKR FHA:DICER WT, N1, ΔHEL1, ΔHEL2i and ΔHEL2, infected at an MOI of 2 for 12h (left) or 16h (right) from plaque assay quantification (n = 3 biological replicates). Ordinary one-way ANOVA test with Dunnett's correction. **: $p < 0.01$; ***: $p < 0.001$; ****: $p < 0.0001$; ns: non-significant.

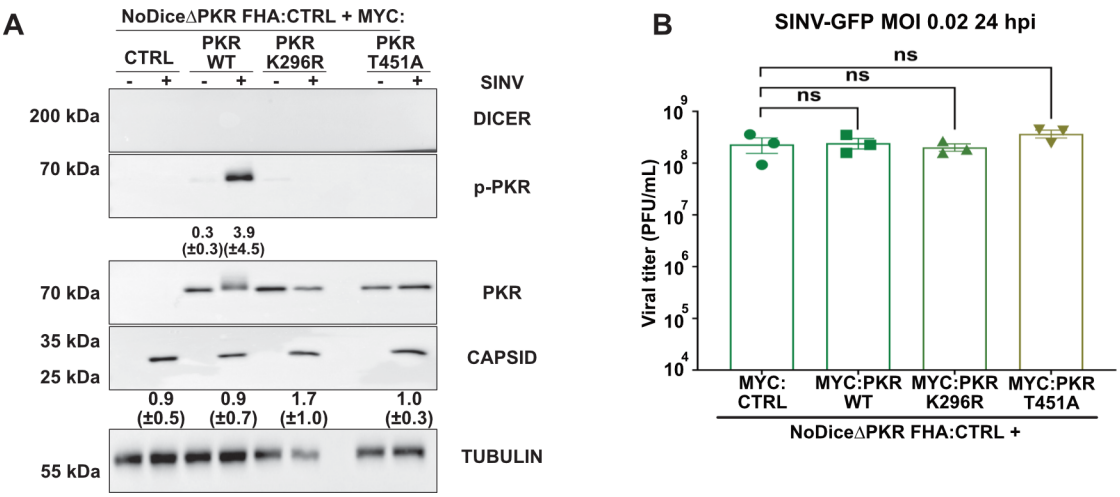

Figure EV3. PKR dimerization and/or catalytic activities do not change the infection outcome in NoDiceΔPKR FHA:CTRL cells

A. Western blot analysis of DICER, p-PKR, PKR and CAPSID expression in SINV-GFP infected NoDiceΔPKR FHA:CTRL cells expressing MYC:EMPTY CTRL vector, MYC:PKR, MYC K296R or MYC:T451A at an MOI of 0.02 for 24h. Alpha-Tubulin was used as loading control. Band intensity was quantified and normalized to Tubulin for three independent biological replicates, then represented as mean (+/- SD) under the corresponding lane; p-PKR = p-PKR/PKR quantification. **B.** Mean (+/- SEM) of SINV-GFP viral titers in the same samples as in A, infected at an MOI of 0.02 for 24h (n = 3 biological replicates) from plaque assay quantification. Ordinary one-way ANOVA test with Dunnett's correction. ns: non-significant.

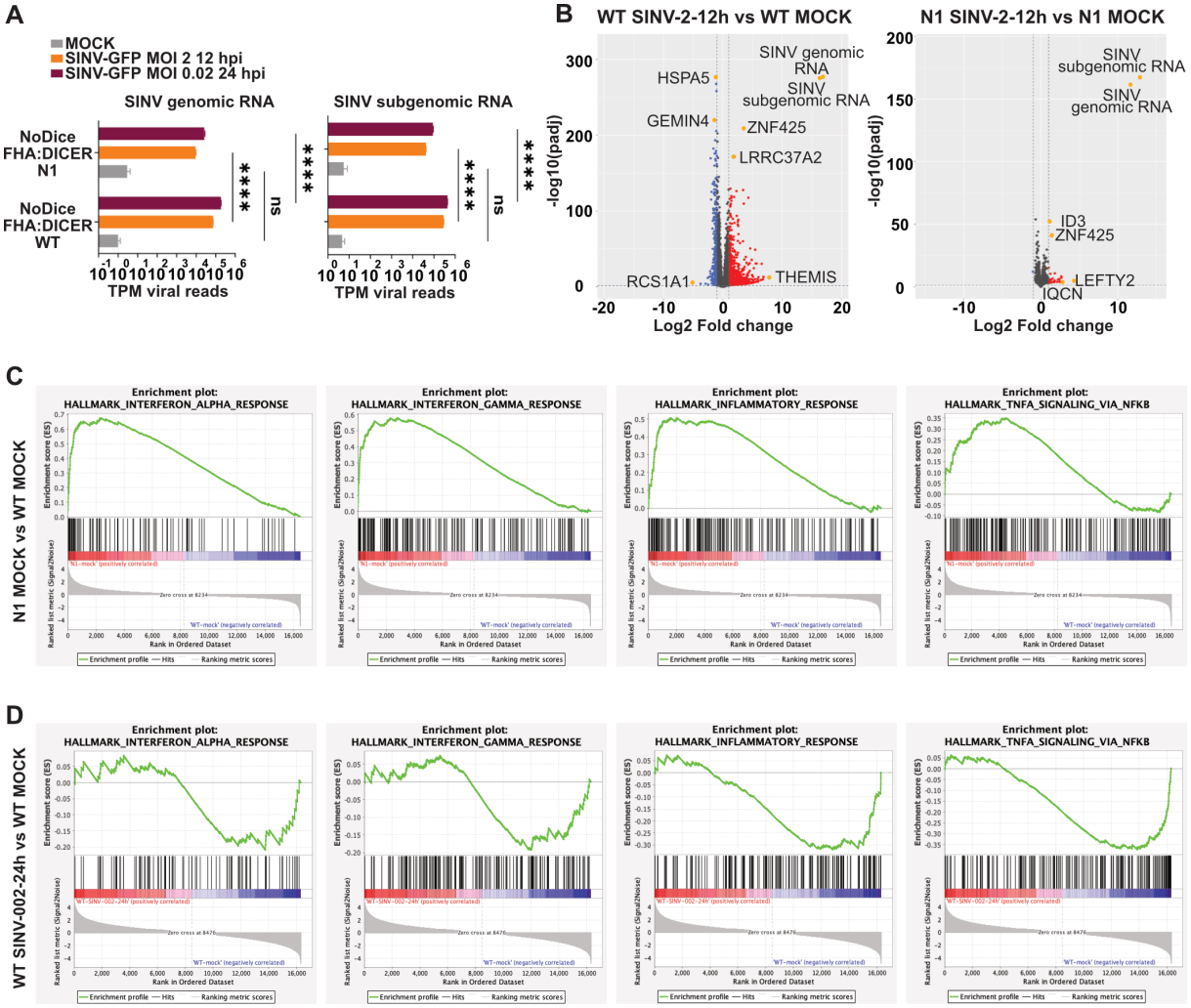

Figure EV4. Dicer N1 cells express a different gene set from Dicer WT cells

A. SINV-GFP genomic and subgenomic read distribution detected by RNA-sequencing analysis in NoDice FHA:DICER WT or N1 cells uninfected (NI, grey) or infected at an MOI of 2 for 12h (orange) or 0.02 for 24h (purple). The viral reads number (mean +/- SEM) is normalized to the total mapped reads in each condition. TPM: transcripts per million. Ordinary two-way ANOVA test with Sidak's correction. ****: $p < 0.0001$; ns: non-significant. (n = 3 biological replicates). **B.** Volcano plots showing for each gene the log2 fold change and adjusted p value (Wald test, DESeq2 package) between SINV-infected (MOI of 2 for 12h) and mock NoDice FHA:DICER WT cells (left), or SINV-infected and mock NoDice FHA:DICER N1 cells (right). Each gene is marked as a dot (red: upregulated, blue: downregulated, grey: unchanged). The horizontal line denotes an adjusted p-value of 0.05 and the vertical ones the Log2 fold change cut-off (-1 and 1). (n = 3 biological replicates). **C-D**, GSEA enrichment plots for selected biological states and processes linked to inflammatory and antiviral pathways for mock NoDice FHA:DICER N1 vs mock NoDice FHA:DICER WT (C), or SINV-infected (MOI of 0.02 for 24h) vs. mock NoDice FHA:DICER WT cells (D).

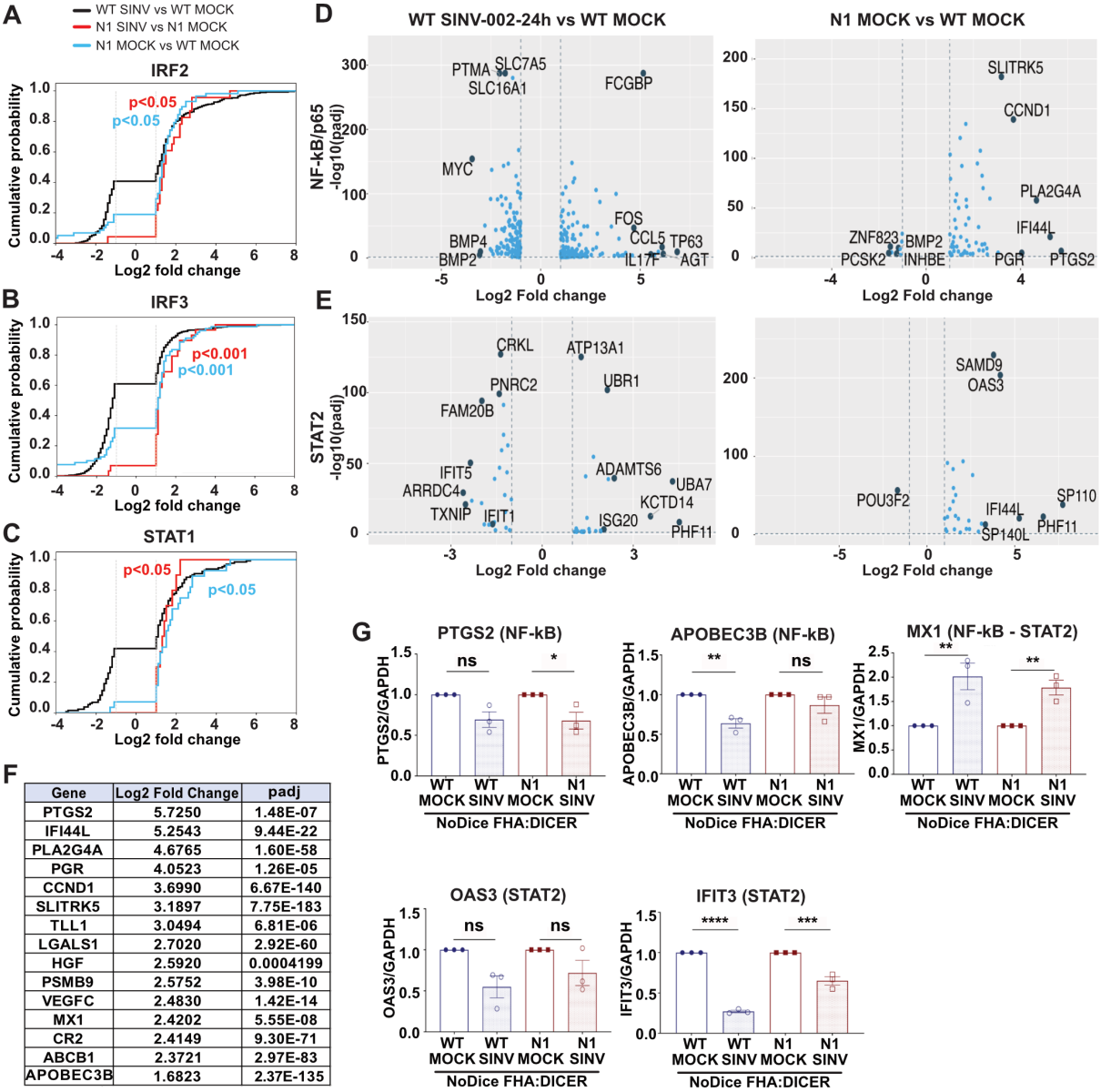

F

Gene	Log2 Fold Change	padj
PTGS2	5.7250	1.48E-07
IFI44L	5.2543	9.44E-22
PLA2G4A	4.6765	1.60E-58
PGR	4.0523	1.26E-05
CCND1	3.6990	6.67E-140
SLITRK5	3.1897	7.75E-183
TLL1	3.0494	6.81E-06
LGALS1	2.7020	2.92E-60
HGF	2.5920	0.0004199
PSMB9	2.5752	3.98E-10
VEGFC	2.4830	1.42E-14
MX1	2.4202	5.55E-08
CR2	2.4149	9.30E-71
ABCB1	2.3721	2.97E-83
APOBEC3B	1.6823	2.37E-135

Figure EV5. Immune-related transcription factors activation is involved in the deregulation of Dicer N1 cells mRNAs

A-C. Histograms representing the cumulative probability of differentially expressed genes controlled by the transcription factors IRF2 (A), IRF3 (B) or STAT1 (C), plotted according to their Log2 fold change. The vertical lines stand for the Log2 fold change cut-offs (-1 and 1). The two-sample Kolmogorov-Smirnov test was used to assess whether each distribution was statistically different from the distribution of NoDice FHA:DICER WT cells infected with SINV vs. mock. p-values are indicated on each histogram. Black: WT SINV-002-24h vs WT MOCK; red: N1 SINV-002-24h vs N1 MOCK; blue: N1 MOCK vs WT MOCK. **D-E.** Volcano plots for differentially expressed genes (DEGs) under the control of NF-kB/p65 (D) or STAT2 (E). Each gene is marked as a dot and plotted based on its log2 fold change and adjusted p values (Wald test, DESeq2 package) comparing SINV-infected (MOI of 0.02 for 24h) vs mock NoDice FHA:DICER WT cells (left), or mock NoDice FHA:DICER WT vs mock NoDice FHA:DICER N1 cells (right). The horizontal line denotes an adjusted p-value of 0.05 and the vertical ones the Log2 fold change cut-offs (-1 and 1). **F.** Table of 15 representative upregulated NF-kB/p65 targets from the DEGs in the comparison mock NoDice FHA:DICER N1 vs mock NoDice FHA:DICER WT. Classification was made according to their Log2 fold change values.

1521 padj: adjusted p-value (Wald test, DESeq2 package). **G.** RT-qPCR on selected DEGs controlled
1522 by either NF-kB/p65 or STAT2 in NoDice FHA:DICER WT and N1 cells infected or not with
1523 SINV-GFP at an MOI of 0.02 for 24h. Mean (+/- SEM); n = 3 biological replicates. One-way
1524 ANOVA with Sidak's correction. *: $p < 0.05$; **: $p < 0.01$; ***: $p < 0.001$; ****: $p < 0.0001$;
1525 ns: non-significant.
1526